The rheology of a semi-dilute suspension of swimming model micro-organisms

TAKUJI ISHIKAWA and T. J. PEDLEY

Journal of Fluid Mechanics / Volume 588 / October 2007, pp 399 - 435
DOI: 10.1017/S0022112007007835, Published online: 24 September 2007

J. Fluid Mech. (2007), *vol.* 588, *pp.* 399–435.
doi:10.1017/S0022112007007835 Printed in the United Kingdom

The rheology of a semi-dilute suspension of swimming model micro-organisms

TAKUJI ISHIKAWA[1] AND T. J. PEDLEY[2]

[1]Department of Bioengineering and Robotics, Tohoku University, 6-6-01, Aoba, Aramaki, Aoba-ku, Sendai 980-8579, Japan

[2]Department of Applied Mathematics and Theoretical Physics, University of Cambridge, Centre for Mathematical Sciences, Wilberforce Road, Cambridge CB3 0WA, UK

(Received 12 September 2006 and in revised form 27 May 2007)

The rheological properties of a cell suspension may play an important role in the flow field generated by populations of swimming micro-organisms (e.g. in bioconvection). In this paper, a swimming micro-organism is modelled as a squirming sphere with prescribed tangential surface velocity, in which the centre of mass of the sphere may be displaced from the geometric centre (*bottom-heaviness*). Effects of inertia and Brownian motion are neglected, because real micro-organisms swim at very low Reynolds numbers but are too large for Brownian effects to be important. The three-dimensional movement of 64 identical squirmers in a simple shear flow field, contained in a cube with periodic boundary conditions, is dynamically computed, for random initial positions and orientations. The computation utilizes a database of pairwise interactions that has been constructed by the boundary element method. The restriction to pairwise additivity of forces is expected to be justified if the suspension is semi-dilute. The results for non-bottom-heavy squirmers show that the squirming does not have a direct influence on the apparent viscosity. However, it does change the probability density in configuration space, and thereby causes a slight decrease in the apparent viscosity at $O(c^2)$, where c is the volume fraction of spheres. In the case of bottom-heavy squirmers, on the other hand, the stresslet generated by the squirming motion directly contributes to the bulk stress at $O(c)$, and the suspension shows strong non-Newtonian properties. When the background simple shear flow is directed vertically, the apparent viscosity of the semi-dilute suspension of bottom-heavy squirmers becomes smaller than that of inert spheres. When the shear flow is horizontal and varies with the vertical coordinate, on the other hand, the apparent viscosity becomes larger than that of inert spheres. In addition, significant normal stress differences appear for all relative orientations of gravity and the shear flow, in the case of bottom-heavy squirmers.

1. Introduction

The size of individual micro-organisms is often much smaller than that of the flow field of interest, in an oceanic plankton bloom for instance. In such cases, the suspension of micro-organisms is modelled as a continuum in which the variables are volume-averaged quantities (Pedley & Kessler 1992; Metcalfe, Pedley & Thingstad 2004). Continuum models for suspensions of swimming micro-organisms have been proposed for the analysis of phenomena such as bioconvection (e.g. Childress, Levandowsky & Spiegel 1975; Pedley & Kessler 1990; Hillesdon, Pedley & Kessler

1995; Bees & Hill 1998; Metcalfe & Pedley 2001). However, the continuum models proposed so far are restricted to dilute suspensions, in which cell–cell interactions are negligible. If one wishes to analyse larger cell concentrations, for example in the dense falling plumes that form part of bioconvection patterns (Kessler *et al.* 1994; Metcalfe & Pedley 2001), it will be necessary to consider the interactions between micro-organisms. Then the particle stress tensor, as well as the velocities of the micro-organisms and the diffusion tensor, in the continuum model will need to be replaced by improved expressions.

In the ocean, the volume fraction of micro-organisms is in general small. Even in red tides, which are caused by more than 200 kinds of phytoplankton, the minimum quantitative standard to define a red tide is approximately 1000 cells per millilitre for rather large flagellates at a diameter of about 30 μm. This density corresponds to a volume fraction of about 0.001 %. However, the volume fraction can be much greater in particular circumstances, for example near an air interface. On the laboratory scale, much higher concentrations are often used. For example, Kessler has used algal cells of the genera *Dunaliella* and *Chlamydomonas* in his experiments (Kessler 1985*a*, 1985*b*, 1986*a*, 1986*b*). These have a mean diameter in the range 10–20 μm. The average volume fraction used in Kessler's experiments was about 0.1 %, but the suspension became much denser locally because of the migration of cells.

Recently Dombrowski *et al.* (2004) have reported a mesoscale structure in a dense suspension of *Bacillus subtilis*, with a volume fraction up to 30 %. In such a dense suspension, it is observed that a *B. subtilis* cell tends to swim in the same direction as its neighbours, and this generates a flow pattern larger than the scale of an individual cell but smaller than the scale of the container used in the experiment. The mesoscale structure changes its direction randomly in a manner reminiscent of turbulence, so Dombrowski *et al.* named this phenomenon *slow turbulence*. Mendelson *et al.* (1999) also observed a mesoscale motion of whorls and jets generated by *B. subtilis* in a thin water film above an agar gel plate.

In all these examples, cell–cell interactions change the swimming motions of individual cells and presumably, therefore, also affect the rheological properties of a suspension of cells. Since the volume fractions of suspensions of plankton, as opposed to the above bacterial experiments, are generally not very great, the bulk effects of cell–cell interactions are likely to be moderate and the assumption of *semi-diluteness* is reasonable.

The model micro-organism used in this paper is the *spherical squirmer* used by Ishikawa, Simmonds & Pedley (2006) in an investigation of all possible hydrodynamic interactions between pairs of cells. Details of a squirmer were given in that earlier paper, so only a brief explanation will be made here. A squirmer has a spherical shape, with prescribed surface tangential velocities given by equation (2.4) below. It is assumed to be neutrally buoyant, because the sedimentation velocities for typical aquatic micro-organisms are much less than the swimming speeds, which range up to several hundred $\mu\mathrm{m\,s^{-1}}$. The centre of buoyancy of the sphere may not coincide with its geometric centre. The model micro-organism is, therefore, force-free but may not be torque-free. The Reynolds number based on the swimming speed and the radius of individuals is usually less than 10^{-2}, so the flow field around the micro-organisms is assumed to be Stokes flow. Brownian motion is not taken into account, because typical micro-organisms are too large for Brownian effects to be important. The model of a squirmer was first proposed by Lighthill (1952), and his analysis was then extended by Blake (1971) and by Felderhof & Jones (2004). A particularly simple way of calculating the swimming speed was given by Stone & Samuel (1996). The

model has also been used by Magar, Goto & Pedley (2003) to analyse nutrient uptake properties of a solitary squirmer.

For any concentration of particles, there is a relation between the deviatoric part of the bulk stress and the conditions at the surfaces of individual particles. This relation was derived by Batchelor (1970) as

$$\boldsymbol{\Sigma} = IT + 2\mu\boldsymbol{E} + \boldsymbol{\Sigma}^{(p)}, \tag{1.1}$$

where IT stands for an isotropic term, μ is the viscosity and $\boldsymbol{E}$ is the bulk rate of strain tensor. $\boldsymbol{\Sigma}^{(p)}$ is the particle bulk stress, and by using the volume, rather than ensemble, average the particle bulk stress caused by force- and torque-free particles in a fluid occupying volume V can be expressed as

$$\boldsymbol{\Sigma}^{(p)} = \frac{1}{V}\sum \boldsymbol{S}, \tag{1.2}$$

where $\boldsymbol{S}$ is the *stresslet* of a single particle and the sum is over all particles. The stresslet is defined to give no isotropic contribution for rigid particles as (Batchelor & Green 1972*b*)

$$\boldsymbol{S} = \int_{A_p} \left[\tfrac{1}{2}\left\{(\boldsymbol{\sigma}\cdot\boldsymbol{n})\,\boldsymbol{x} + \boldsymbol{x}\,(\boldsymbol{\sigma}\cdot\boldsymbol{n})\right\} - \tfrac{1}{3}\boldsymbol{x}\cdot\boldsymbol{\sigma}\cdot\boldsymbol{n}\boldsymbol{I} - \mu\,(\boldsymbol{u}\boldsymbol{n} + \boldsymbol{n}\boldsymbol{u})\right] \mathrm{d}A, \tag{1.3}$$

where $\boldsymbol{\sigma}$ is the stress tensor and $\boldsymbol{u}$ is the velocity. The surface of each particle is defined as A_p with an outward normal vector $\boldsymbol{n}$. The stresslet for a solitary squirmer ($\boldsymbol{S}_{sol}$) was shown by Ishikawa *et al.* (2006) to be

$$\boldsymbol{S}_{sol} = \frac{4\pi}{3}\mu a^2(3\,\boldsymbol{e}\boldsymbol{e} - \boldsymbol{I})B_2, \tag{1.4}$$

where a is the radius, $\boldsymbol{e}$ is the orientation vector of the squirmer and B_n is the nth mode of the surface squirming velocity; see (2.4). This stresslet gives the first-order correction to the bulk stress in terms of the volume fraction c. That axisymmetric swimming micro-organisms would generate a stresslet of this form was also noted by Pedley & Kessler (1990) and by Hatwalne *et al.* (2004).

The next term in the asymptotic expression for the particle bulk stress in terms of c is of $O(c^2)$, as shown by Batchelor & Green (1972*a*, *b*), who were able to provide a method of calculating this term for non-Brownian hard spheres in a simple straining flow field. The critical function here was the conditional probability density function that the spheres are in a given configuration ζ_N given that there is an *additional* sphere centred at $\boldsymbol{x}_0$, $P(\zeta_N|\,\boldsymbol{x}_0)$ (N particles are assumed to be in the volume V). If one applies this method to a suspension of squirmers, one needs to introduce the conditional probability that N squirmers are in a configuration ζ'_N given that there is an additional squirmer centred at $\boldsymbol{x}_0$ with orientation vector $\boldsymbol{e}_0$, denoted by $P(\zeta'_N|\,\boldsymbol{x}_0, \boldsymbol{e}_0)$. The correction to the particle stress is then

$$\frac{1}{N!}\int \{\boldsymbol{S}(\boldsymbol{x}_0, \boldsymbol{e}_0, \zeta'_N) - \boldsymbol{S}_{sol}\} P(\zeta'_N|\,\boldsymbol{x}_0, \boldsymbol{e}_0)\,\mathrm{d}\zeta'_N, \tag{1.5}$$

where $\boldsymbol{S}(\boldsymbol{x}_0, \boldsymbol{e}_0, \zeta'_N)$ is the stresslet of the squirmer centred at $\boldsymbol{x}_0$ with the orientation of $\boldsymbol{e}_0$, while the other N squirmers are in the configuration ζ'_N. The governing equation for the probability density function is given by a Fokker–Planck equation with zero diffusion, and it was analytically solved by Batchelor & Green (1972*b*) for the inert sphere case. Rather than replicating this calculation for a suspension of squirmers, we will use a completely different method to solve the next order effect on the particle

bulk stress. This is because solving the Fokker–Planck equation with zero diffusion presents a number of difficulties.

(*a*) The Fokker–Planck equation for the probability density of two squirmers depends on the relative position and the orientations of the two squirmers and, therefore, it becomes a nine-dimensional function instead of the three-dimensional function required for inert spheres.

(*b*) Even the Fokker–Planck equation for the probability density of two inert spheres could not be solved when the background flow is a simple shearing motion because of the existence of closed trajectories (Batchelor & Green 1972*b*).

(*c*) Analytical results for the Fokker–Planck equation with zero diffusion are not available and numerical methods to deal strictly with zero diffusion are not available either.

A lot of work has been done to analyse the rheological properties of a suspension of inert spheres in a Stokes flow regime, a field that was pioneered by Batchelor (1970). Brady and his colleagues have calculated the particle stress tensor in a simple shear flow and in a pressure-driven flow by using Stokesian-dynamics simulations (Brady & Bossis 1988; Nott & Brady 1994). Numerical methods for Stokesian-dynamics simulations of a finite number of particles are explained by Durlofsky, Brady & Bassis (1987), and those for an infinite number of particles are explained by Brady *et al.* (1988). Here we use an early version of Stokesian dynamics that was also proposed by Brady, based on pairwise additivity in constructing a grand resistance matrix (Brady & Bossis 1985; Bossis & Brady 1984). This method is suitable for a semi-dilute suspension, in which most of the interactions are pairwise, and is easy to extend to a suspension of squirmers. The pairwise additivity is an approximation, but it is expected to be justified if the particle volume fraction is not too large (defining *semi-dilute*). Because the contribution of a solitary particle to the bulk stress is the order of c, the contribution of two-particle interactions is of order c^2, and the contribution of interactions between three or more particles is of order c^3 (Batchelor & Green 1972*b*). We seek to calculate the $O(c)$ and $O(c^2)$ terms. The details of our numerical methods will be explicitly described in § 2. We use the term *semi-dilute* because the suspension investigated in this study is not dilute enough to neglect interactions between particles nor dense enough that many-body interactions cannot be approximated in a pairwise additive fashion.

Hydrodynamic interactions between micro-organisms have been investigated by other researchers (Guell *et al.* 1988; Ramia, Tullock & Phan-Thien 1993; Nasseri & Phan-Thien 1997; Lega & Passot 2003; Jiang, Osborn & Menevean 2002), but none of them studied two micro-organisms in near-contact. Mehandia & Nott (2004) have simulated two-dimensional collective motions of 80 model micro-organisms by assuming that the model has a spherical shape with a constant force dipole. The assumption of a constant force dipole is acceptable when the distance between particles is large enough. When two of them are in near-contact, however, this assumption may not be true, because the stresslet is the resultant of the change in the velocity field and should be obtained as part of the solution to the problem. The effect of the interaction between micro-organisms on the rheological properties of the suspension has also not been discussed before. To perform such an investigation, it is sensible to begin by considering passive hydrodynamic interactions, in which the micro-organisms do not actively react to the presence of others. Throughout this paper the squirming motion of a sphere's surface is assumed to be invariant.

In this paper, the three-dimensional movement of 64 identical squirmers in a simple shear flow field, contained in a cube with periodic boundary conditions, is

dynamically computed, for random initial positions and orientations. In order to include the cell–cell interactions, we use a database of pairwise interactions that has previously been constructed by a boundary element method (Ishikawa *et al.* 2006). In § 3, the rheological properties of a semi-dilute suspension of *non-bottom-heavy* squirmers will be investigated. When squirmers are non-bottom-heavy, there is no preferred direction. Thus the average stresslet of the squirmers should be isotropic, which results in no direct contribution to the apparent viscosity of the suspension. The interaction between squirmers, however, changes the probability density of the configuration, and eventually it changes the apparent viscosity indirectly. The effect of volume fraction and mode of squirming on the apparent viscosity will be discussed in this section. In § 4, the rheological properties of a semi-dilute suspension of *bottom-heavy* squirmers will be investigated. When squirmers are bottom-heavy, gravity exerts an external torque, which generates an asymmetric contribution to the bulk stress tensor. Therefore, the bulk stress tensor shows strong non-Newtonian behaviour. Moreover, bottom-heavy squirmers tend to swim upwards, so there is a preferred direction. The squirmers' stresslet in this case is no longer isotropic, which also results in a direct contribution to the apparent viscosity and normal stress differences of the suspension. The orientation of the background shear flow relative to gravity becomes important. The effect of volume fraction, mode of squirming and the strength of the bottom-heaviness on the bulk stress tensor will be discussed in this section.

2. Numerical methods

The dynamic simulation method, based on pairwise additivity in constructing a grand resistance matrix, can be found in Brady & Bossis (1985) and Bossis & Brady (1984). The numerical method used in this study is similar to theirs, but we had to modify the method in order to deal with a suspension of squirmers instead of a suspension of inert spheres. We will mainly use the same notation as in Brady & Bossis (1985).

In the absence of Brownian motion and at negligible particle Reynolds number, the equation of motion for N identical squirmers suspended in a Newtonian solvent undergoing a bulk linear shear flow can be written as

$$-\boldsymbol{R}\cdot\boldsymbol{U}^{*}+\boldsymbol{\Phi}:\boldsymbol{E}+\boldsymbol{F}_{sq}+\boldsymbol{F}_{tor}+\boldsymbol{F}_{rep}=0. \tag{2.1}$$

Here $\boldsymbol{U}^{*}$ is a vector of dimension $6N$ containing the translational-rotational velocities of the N particles relative to the bulk fluid's velocities evaluated at the squirmer centre. $\boldsymbol{R}$ is the grand resistance matrix of dimension $6N\times 6N$, which is constructed by a pairwise superposition of exact results for two inert spheres. The $6N\times 3\times 3$ matrix $\boldsymbol{\Phi}$ gives the force–torque on the squirmers due to the bulk shear flow, which is also constructed by a pairwise superposition of exact two-sphere results. Exact solutions of the force–torque on two inert spheres are included in standard texts (e.g. Kim & Karrila 1992). For simple shear in the x,y-plane, the bulk rate of strain tensor $\boldsymbol{E}$ is given by

$$\boldsymbol{E}=\frac{\dot{\gamma}}{2}\begin{pmatrix}0&1&0\\1&0&0\\0&0&0\end{pmatrix}, \tag{2.2}$$

where $\dot{\gamma}$ is the shear rate. The bulk vorticity $\boldsymbol{\Omega}$ is

$$\boldsymbol{\Omega}=-\frac{\dot{\gamma}}{2}(0,0,1). \tag{2.3}$$

$\boldsymbol{F}_{sq}$ is the force–torque due to the squirming motion on the surface of spherical particles without any translational–rotational motion. It is calculated from superposition of pairwise interactions between squirmers, in which translational and rotational motions are restrained, using the boundary element method (cf. Ishikawa *et al.* 2006). We should note that two nearby squirmers generate high multipoles even though they generate only stresslet when they are alone. Such high multipoles are included in $\boldsymbol{F}_{sq}$, because they can be calculated by the boundary element method. $\boldsymbol{F}_{tor}$ consists of the external torques due to the bottom-heaviness, and $\boldsymbol{F}_{rep}$ contains the non-hydrodynamic interparticle forces (if any). The details of $\boldsymbol{F}_{sq}$, $\boldsymbol{F}_{tor}$ and $\boldsymbol{F}_{rep}$ will be described explicitly later in this section. The first term in (2.1) represents the force–torque generated on inert spheres due to their translational–rotational motion in a fluid otherwise at rest. The second term represents the force–torque on inert spheres, without translational–rotational motion, due to the background linear flow field. The third term represents the force–torque on squirmers, without translational–rotational motion, due to their surface squirming motions. These three terms are hydrodynamic forces–torques, and it is possible to exploit the linearity of the Stokes equation to decompose the total hydrodynamic force into the three simpler hydrodynamic forces.

The surface of a spherical squirmer is assumed to move purely tangentially and these tangential motions are assumed to be axisymmetric and time-independent. Thus the tangential surface velocity on a squirmer is given as

$$\boldsymbol{u}_s = \sum_{n=1}^{2} \frac{2}{n(n+1)} B_n \left(\frac{\boldsymbol{e}\cdot\boldsymbol{r}}{r}\frac{\boldsymbol{r}}{\boldsymbol{r}} - \boldsymbol{e} \right) P_n'(\boldsymbol{e}\cdot\boldsymbol{r}/r), \tag{2.4}$$

where P_n is the nth Legendre polynomial, $\boldsymbol{r}$ is the position vector and $r = |\boldsymbol{r}|$. We follow Ishikawa *et al.* (2006) and omit all squirming modes higher than the second, i.e. $B_n = 0$ in $\boldsymbol{u}_s$ when $n \geqslant 3$. The reasons for limiting ourselves to the first and second modes are as follows.

(i) In the case of a solitary squirmer, the first mode determines the swimming speed, the second mode determines the stresslet, and the higher modes have no effect on the swimming speed or the stresslet.

(ii) The higher a mode is, the more rapidly it decays with r, so the effect of higher modes is negligible in the far-field interaction.

(iii) The role of high modes in the near-field is to generate fluctuations in the velocities and stresslet due to small displacements in the θ-direction.

The overall properties should be captured by using the first two modes. This simplification in the boundary condition will be used throughout this paper. We let the ratio of second-mode squirming to first-mode squirming be β, i.e. $\beta = B_2/B_1$. It should be noted that B_2, and hence β, can have either sign. A squirmer with positive β is a *puller*, analogous to a micro-organism for which the thrust-generating apparatus is in front of the body (which dominates the drag), as for biflagellate algae such as *Chlamydomonas*, whereas a squirmer with negative β is a *pusher*, i.e. the thrust is generated behind the body, as for bacteria or spermatozoa. As an example, the velocity field generated by a solitary squirmer with $\beta = 5$ is shown in figure 1. The authors have already compiled a database of pairwise interactions, covering the whole range of relative initial positions and orientations of the two squirmers for various positive values of β (Ishikawa *et al.* 2006) and, more recently, for negative values of β (unpublished) from which an arbitrary interaction can be interpolated. We will exploit the database in constructing $\boldsymbol{F}_{sq}$, which represents the pairwise superposition of the interaction of two squirmers.

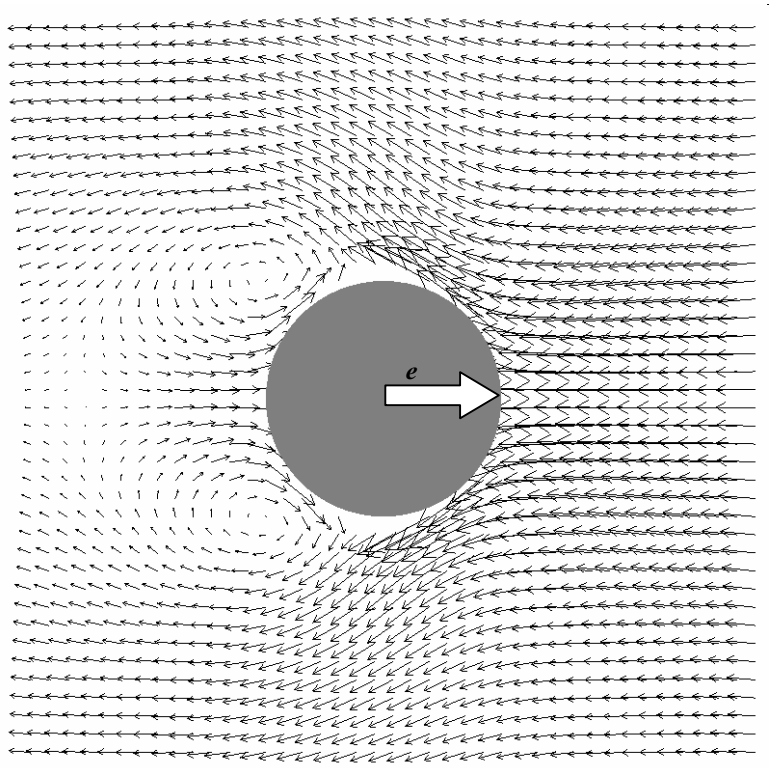

FIGURE 1. Velocity vectors relative to the translational velocity vector of a solitary squirmer with $\beta = 5$. Uniform flow of speed 1.0, in dimension-free form, coming from far right.

If the squirmer is bottom-heavy, there is an external torque acting on the squirmer and this must be equal to the hydrodynamic torque, so that the net torque on the squirmer is zero. If the distance of the centre of gravity is h from the centre of the squirmer, in the opposite direction to its swimming direction in undisturbed fluid (see figure 2), then there is an additional torque of

$$\boldsymbol{F}_{tor} = \tfrac{4}{3}\pi a^3 \rho h \boldsymbol{e} \wedge \boldsymbol{g}, \tag{2.5}$$

where ρ is the density, $\boldsymbol{g}$ is the gravitational acceleration vector, and the gravitational direction is $\boldsymbol{g}/g$.

Although the governing equation of squirmer motions (2.1) does not in principle allow the spheres to overlap, there are cases of very small separation in which numerical errors associated with the integration of $\boldsymbol{U}^*$ in time can lead to an apparent overlap. In order to avoid the prohibitively small time step needed to overcome this problem, we introduce a repulsive force, as used by Brady & Bossis (1985, 1988):

$$\boldsymbol{F}_{rep} = \alpha_1 \frac{\alpha_2 \exp(-\alpha_2 \varepsilon)}{1 - \exp(-\alpha_2 \varepsilon)} \frac{\boldsymbol{r}}{r}, \tag{2.6}$$

where α_1 is a dimensional coefficient, α_2 is a dimensionless coefficient and ε is the minimum separation between squirmer surfaces non-dimensionalized by their radius. This form of the interparticle force corresponds to charged particles interacting through colloidal forces at constant surface charge. Dratler & Schowalter (1996) employed two completely different types of repulsive forces for their dynamic simulation of suspensions of non-Brownian hard spheres, and concluded that the precise form of the repulsive force is unimportant provided it decays rapidly to zero with increasing particle separation. The coefficients used in this study are

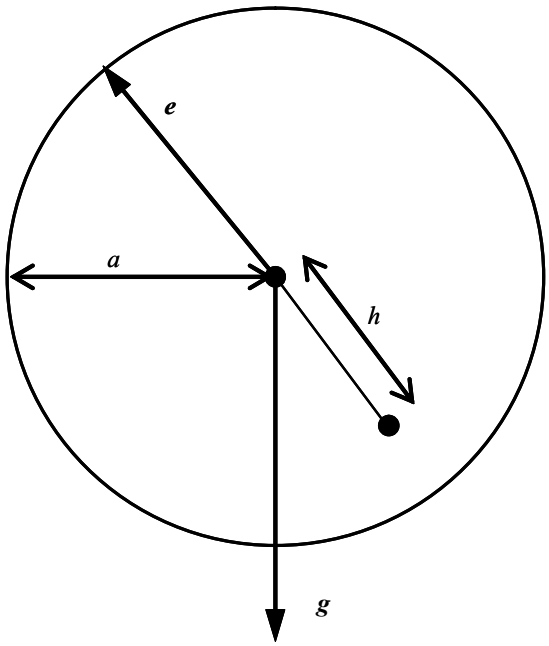

FIGURE 2. A sketch of the arrangement of a bottom heavy squirmer. Gravity acts in the $\boldsymbol{g}$-direction, while the squirmer has orientation vector $\boldsymbol{e}$, radius a and its centre of mass distance h from its geometrical centre.

$\alpha_1/(\mu a^2\dot{\gamma}) = 10^{-2} - 10^{-4}$ and $\alpha_2 = 10^3$. The minimum separation obtained with these parameters is in the range $10^{-4} - 10^{-5}$.

The effect of repulsive forces between inert spheres on the pair distribution function can be found in Bossis & Brady (1984), and that on the rheological properties in Brady & Bossis (1985). In the case of non-bottom-heavy squirmers, the effect of the repulsive forces on the bulk stress is small, because the stresslet due to squirming is isotropic, as will be discussed in § 3. When squirmers are bottom-heavy, the squirming motion directly contributes to the bulk stress. The stresslets generated by the squirming motions of two squirmers in near-field separation were derived analytically using lubrication theory by Ishikawa *et al.* (2006), and the leading order of the stresslet is $\log(\varepsilon^{-1})$. Therefore the bulk stress due to squirming diverges if ε goes to zero, and the effect of the repulsive force cannot be formally neglected. Fortunately, however, the leading order term $\log(\varepsilon^{-1})$ is a very weak singularity, and thus dominates the solution only in a mathematical sense. Even if we take ε as the ratio of molecular to macroscopic dimensions, $\log \varepsilon^{-1}$ is not large enough to generate a strong stresslet. Thus, the repulsive force does not significantly affect the stresslet due to squirming provided that ε is taken as the dimensionless size of a molecule or larger.

The bulk rheological properties of a suspension can be described by the average stress tensor. In the presence of external torques due to bottom-heaviness and interparticle forces, there are two contributions to the bulk stress: (i) particle contribution to the hydrodynamic stress due entirely to the bulk deformation imposed at the outer boundary, and (ii) particle contribution to the elastic stress due to the repulsive forces. Batchelor (1977) derived the particle bulk stress as

$$\boldsymbol{\Sigma}^{(p)} = \frac{1}{V}\sum_{N} \boldsymbol{H} = \frac{1}{V}\sum_{N}\{\boldsymbol{S} + \boldsymbol{S}' + \boldsymbol{J}\}, \tag{2.7}$$

where $\boldsymbol{S}$ is the stresslet given by (1.3), $\boldsymbol{S}'$ is the asymmetric part of the force dipole generated by the external torques, $\boldsymbol{J}$ is the elastic stress and $\boldsymbol{H}$ is the total stress.

It is possible to exploit the linearity of the Stokes equation to decompose the total hydrodynamic stress into simpler stresses. These stresses are calculated in a pairwise additive fashion, in a similar manner to the force and torque. The stresslet due to squirming motions is obtained from our database of pairwise interactions. The stress due to external torques ($\boldsymbol{S}'$) can be calculated by (cf. Kim & Karrila 1992)

$$\boldsymbol{S}' = -\frac{1}{2}\boldsymbol{\epsilon} : \boldsymbol{T}, \tag{2.8}$$

where $\boldsymbol{\epsilon}$ is the unit alternating isotropic tensor, and $\boldsymbol{T}$ is the external torque. The torque due to bottom-heaviness has already been given by (2.5). This stress has no interaction with other squirmers, so it can be calculated individually. The elastic contribution to the particle bulk stress $\boldsymbol{J}$ can be calculated as (Batchelor 1977)

$$\sum_{N} \boldsymbol{J} = -\sum_{i=2}^{N} \sum_{j<i} \boldsymbol{r}^{ij} \boldsymbol{F}^{ij}, \tag{2.9}$$

where $\boldsymbol{r}^{ij}$ is the centre–centre separation of squirmers i and j, and $\boldsymbol{F}^{ij}$ is their pairwise interparticle force given by (2.6).

The computational region is a cube with side L. The background simple shear flow is in the x, y-plane as given by (2.2) and (2.3). To model a suspension of infinite extent, periodic boundary conditions are employed, as used by Brady & Bossis (1985) and Bossis & Brady (1984). For the simple shear flow in the x,y-plane, the periodic conditions in the x- and z-directions are straightforward. In the y-direction, however, the periodicity requires a translation in the x-direction by an amount $L\dot{\gamma}t$ in order to preserve the bulk linear shear flow, where t is time. In using periodic boundary conditions a squirmer interacts with the other squirmers in the periodic cell, whose centre coincides with the centre of the squirmer of interest, and interactions with particles outside the cell are neglected. Since a squirmer is a force-free particle, the stresslet disturbance due to the particle decays as r^{-3}, where r is the distance. By using Green's theorem for Stokes flow one can show, as O'Brien (1979) has for Laplace's equation, that force-free particles outside a volume of characteristic radius r_c in total contribute zero to the stresslet of a particle at the centre of this volume with an error $O(r_c^{-3})$. The minimum length of L used in this study is about 14, so the maximum error for the stresslet disturbance due to the boundary condition is approximately 0.3 %, which is acceptable. A further check on the accuracy of the computations is made in Appendix A, where the shear viscosity is computed for a periodic suspension on a cubic lattice, and compared with the exact solution of Nunan & Keller (1984). The results agree well for $c < 0.15$.

All equations are non-dimensionalized by using radius a, characteristic velocity $a\dot{\gamma}$ and the fluid viscosity μ. There are two important dimensionless parameters in addition to β: Sq and G_{bh}. Sq is the ratio of the swimming velocity of a solitary squirmer ($2B_1/3$) to the characteristic velocity, and is defined as

$$Sq = \frac{2B_1}{3a\dot{\gamma}}. \tag{2.10}$$

G_{bh} is the ratio of the gravitational torque to a scale for the viscous torque, based on the squirming velocity, and is defined as

$$G_{bh} = \frac{2\pi\rho g a h}{\mu B_1}. \tag{2.11}$$

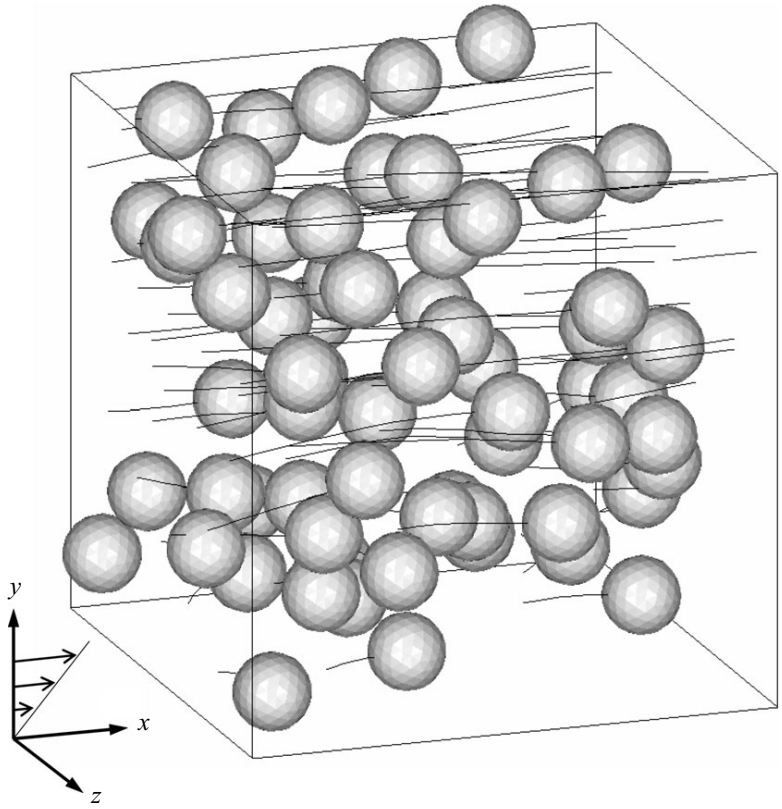

FIGURE 3. Instantaneous position of 64 identical squirmers with $Sq = 1$ and $\beta = 5$. Solid lines are trajectories of the squirmers during one time interval. The background simple shear flow is in the x,y-plane.

The time-marching is performed by the fourth-order Adams–Bashforth scheme. The effect of the number of particles can be found in Bossis & Brady (1984), in which the same numerical methods were employed. They used 25 particles and the accuracy was confirmed by comparing with the results for 100 particles. We have also performed some test calculations with 27, 64 and 125 inert spheres in a simple shear flow field. The results show that the difference between the 64- and 125-particle cases in the averaged stresslet, defined by equation (1.3), is about 1 % or less in our parameter range, so we will use 64 particles as a balance between accuracy and numerical efficiency. Most of the computations will be performed in the time interval of $t = 0 - 100$, and suspension-average values are calculated by averaging all particles in the computational cell from $t = 20$ to 100. It is confirmed that the probability density function of two squirmers becomes independent of specific initial conditions after $t = 20$.

3. A semi-dilute suspension of non-bottom-heavy squirmers

Initially the three-dimensional movement of 64 identical non-bottom-heavy squirmers with $\beta = 5$ in a simple shear flow field is computed under the conditions of $c = 0.1$ and $Sq = 1$. The parameters for the repulsive force (2.6) are $\alpha_1/(\mu a^2 \dot{\gamma}) = 10^{-2}$ and $\alpha_2 = 10^3$. The instantaneous positions of squirmers and their trajectories during one time interval are shown in figure 3, where the background shear flow is in the x,y-plane. Some of the lines in figure 3 are not attached to spheres, because a squirmer passing through a boundary of the periodic cell is replaced on the other side, and its trajectory has a jump at the boundary. Since the background translational velocity

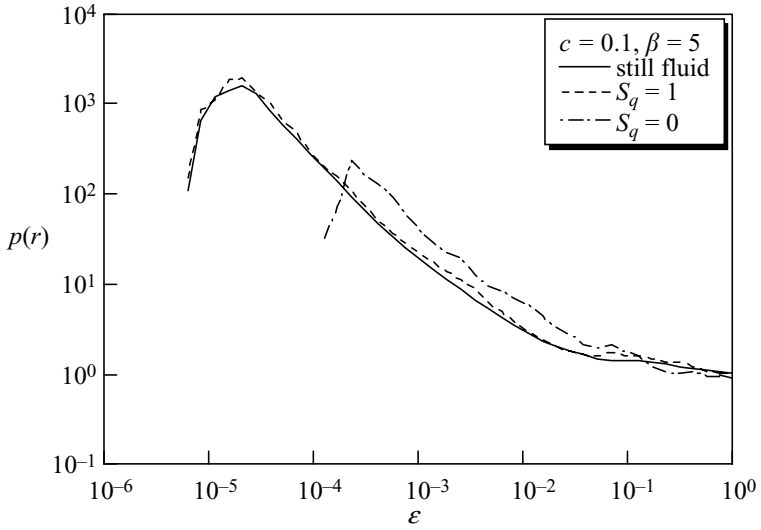

FIGURE 4. Normalized probability density function distribution for $Sq = 1$ and 0 in a shear flow ($c = 0.1$ and $\beta = 5$), where ε is the separation between squirmer surfaces. $Sq = 0$ corresponds to no squirming, i.e. the same as inert spheres. 'Still fluid' stands for the case in which squirmers swim in a still fluid.

increases with y, the trajectories of squirmers in high y positions become longer than those in low y positions. The squirmers in a shear flow cannot swim in straight lines, because they rotate along with the background vorticity and their interactions generate translational–rotational velocities (see Ishikawa *et al.* 2006).

The normalized probability density distribution in this case, defined as

$$p(r) = \frac{\displaystyle\int_{r=\text{const}} P(\boldsymbol{r}_0|\boldsymbol{r}_0 + \boldsymbol{r})\,\mathrm{d}\boldsymbol{r}}{4n\pi r^2}, \tag{3.1}$$

is shown in figure 4; here n is the number density ($n = N/V$), and $P(\boldsymbol{r}_0|\boldsymbol{r}_0 + \boldsymbol{r})\,\mathrm{d}\boldsymbol{r}$ is the conditional probability that, given that there is a squirmer centred at $\boldsymbol{r}_0$, there is an *additional* squirmer centred between $\boldsymbol{r}_0 + \boldsymbol{r}$ and $\boldsymbol{r_0} + \boldsymbol{r} + \mathrm{d}\boldsymbol{r}$. The normalized probability densities in the case of inert spheres in a shear flow ($Sq = 0$) and in the case of squirmers in a still fluid, i.e. $Sq = \infty$, are shown in figure 4 as well. We see that the $p(r)$ distribution for the $Sq = 1$ case is very similar to that for squirmers in a still fluid, so the $p(r)$ in the near-field is dominated by the squirming motion rather than the background shearing motion if $Sq = 1$. The minimum separation in the $Sq = 1$ case about 10^{-5} and in the $Sq = 0$ case about 10^{-4}, which means the minimum separation decreases with increasing squirming motion.

The stresslet generated by two spheres in a shear flow increases with decreasing ε (cf. Kim & Karrila 1992), where ε is the separation between squirmer surfaces. Therefore, the particle stress $\boldsymbol{H}$ may be increased by the squirming motion. On the other hand, $p(r)$ with $Sq = 1$ is smaller than with $Sq = 0$ when $2 \times 10^{-4} \leqslant \varepsilon \leqslant 10^{-1}$. The smaller the $p(r)$ is, the smaller the stresslet generated, so a lower particle stress may be generated in this regime. Which of these two contrary effects dominates the particle stress due to squirming will be of interest.

Since the particle bulk stress is given by (2.7), the apparent viscosity of the suspension may be calculated as

$$\eta = \mu\left(1 + \frac{3}{4\pi}\frac{H_{xy}}{\mu\dot{\gamma}}c\right), \tag{3.2}$$

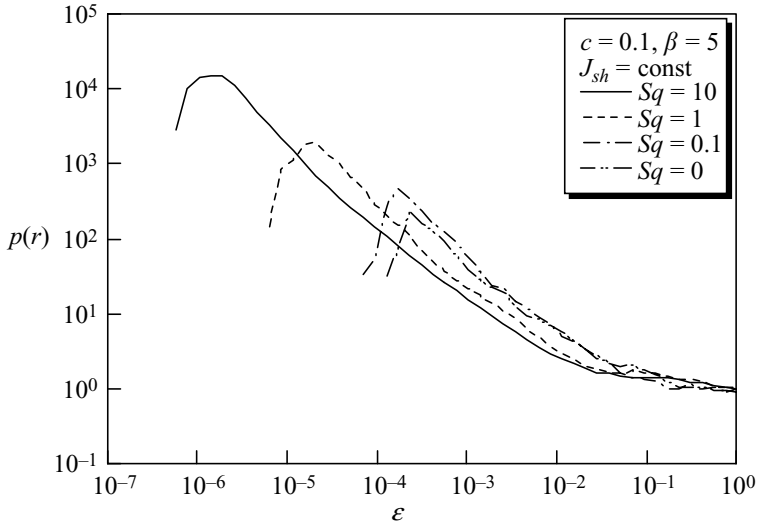

FIGURE 5. Normalized probability density function distribution for $Sq = 0, 0.1, 1$ and 10 ($c = 0.1$ and $\beta = 5$). J_{sh} is kept constant, which corresponds to changing the squirming velocity while the ambient shear rate and the repulsive force between squirmers are kept constant.

and in what follows we will mainly discuss the (x,y)-component of the particle stress, H_{xy}; H_{xy} for $Sq = 1$ is 12.5 and for $Sq = 0$ is 12.8. Therefore, the apparent viscosity is decreased, slightly, by the squirming motion. We may say that the effect of the smaller $p(r)$ in the $2 \times 10^{-4} \leqslant \varepsilon \leqslant 10^{-1}$ regime is stronger than that of the smaller minimum separation. The effect is very small, however. The numerical error of the present simulation associated with the time-averaging process is less than about ± 0.1 for H_{xy}. (Error bars will be shown only when the size of an error bar is wider than the dot representing the data.) It was confirmed numerically that the effect of squirming on H_{xy} exceeds the numerical error, by performing trial simulations with various initial conditions of particles, various particle numbers and various time-intervals for averaging.

The dominant dimensionless parameter for this phenomenon is Sq. However, the squirming effect on the rheological property of the suspension is so small that the effect of the repulsive force cannot be neglected completely. The strength of the repulsive force may be assumed as a physical property for each particle, and is not influenced by the ambient flow field. Thus we introduce the following two dimensionless parameters:

$$J_{sh} = \frac{\alpha_1}{\mu a^2 \dot{\gamma}}, \quad J_{sq} = \frac{3\alpha_1}{2\mu a B_1}. \tag{3.3}$$

J_{sh} is the ratio of the repulsive force to the viscous force due to the background shear flow, and J_{sq} is the ratio of the repulsive force to the viscous force due to the squirming motion. The effect of Sq will be investigated first with J_{sh} kept constant ($\alpha_1/(\mu a^2 \dot{\gamma}) = 10^{-2}$ and $\alpha_2 = 10^3$), which corresponds to changing the squirming velocity while the ambient shear rate and strength of the repulsive force are kept constant. Secondly the effect of Sq will be investigated with J_{sq} held constant ($\alpha_1/(\mu a^2 \dot{\gamma}) = 10^{-2} - 10^{-4}$ and $\alpha_2 = 10^3$), which corresponds to changing the ambient shear rate while the squirming velocity and strength of the repulsive force are kept constant. The effect of changing α_1 will be omitted in the following, because α_1 controls only the minimum separation between squirmer surfaces, and this has a weak effect on the bulk stress, as discussed in § 2.

The normalized probability densities for constant J_{sh} are shown in figure 5 for $Sq = 0$, 0.1, 1 and 10 ($c = 0.1$ and $\beta = 5$). By comparing $Sq = 0$, 1 and 10, we see that

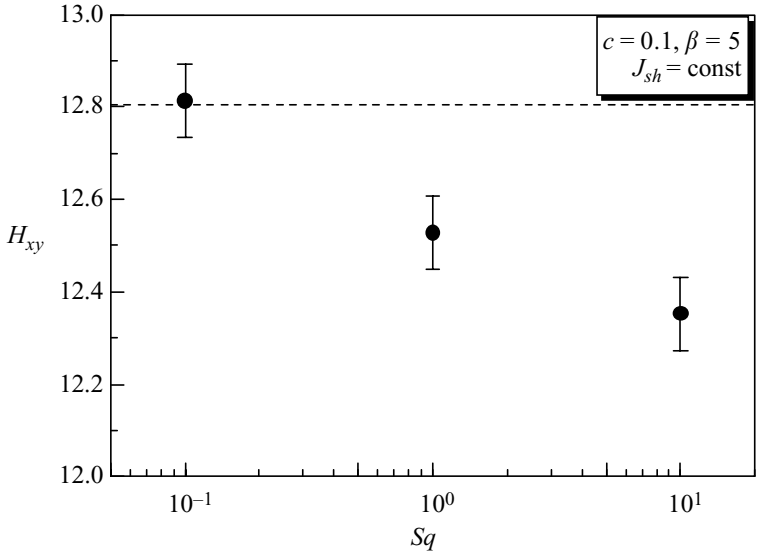

FIGURE 6. Particle stress component H_{xy} under the $J_{sh} = \text{const}$ condition with $Sq = 0, 0.1, 1$ and 10 ($c = 0.1$ and $\beta = 5$). The result of $Sq = 0$ is shown as a broken line.

the minimum separation decreases with increasing Sq, and the value of $p(r)$ decreases in the near-field with increasing Sq. This result is consistent with our former study on the interaction between just two squirmers (Ishikawa *et al.* 2006), in which, in general, two squirmers at first attract each other, then they change their orientation dramatically in the near-field, and eventually avoid each other. Two squirmers can come very close, but they do not swim as a pair (except when the trajectories are confined to two dimensions, which is not being considered here) and avoid each other after a very short period. In the case of two inert spheres in a shear flow, however, there is an infinite region of closed trajectories, in which two spheres remain indefinitely as a pair (Batchelor & Green 1972*a*). This essential difference may be the reason why the $p(r)$ distribution is influenced considerably by Sq. The particle stress component H_{xy} in this case is shown in figure 6 for $Sq = 0$, 0.1, 1 and 10. The result for $Sq = 0$ is shown as a broken line in the figure. It is found that H_{xy} decreases with increasing Sq and hence the squirming motion has the effect of reducing the apparent viscosity of the suspension slightly.

Secondly J_{sq} is kept constant. The normalized probability densities are shown in figure 7 for $Sq = 0.1$, 1 and 10 ($c = 0.1$ and $\beta = 5$). (The inert sphere case was not included because it corresponds to $Sq = \infty$ under the constant J_{sq} condition.) It is found that the minimum separation does not change with Sq, because it is dominated mainly by the squirming motion in this regime and the squirming velocity is kept constant if J_{sq} is kept constant. The effect of the background shear flow is apparent when $Sq = 0.1$; $p(r)$ increases with increasing shear rate for small Sq. If $Sq \geqslant 1$ the $p(r)$ distribution is almost unaffected, because the effect of the background shear flow is too small to overcome the effect of squirming. The particle stress component H_{xy} in this case is shown in figure 8 for $Sq = 0.1$, 1 and 10. It is found that H_{xy} decreases with increasing Sq for small Sq, which is the same tendency as for constant J_{sh}. Here, however, H_{xy} converges to a fixed value if $Sq \geqslant 1$, because the effect of the background shear flow has become too weak.

β is the ratio of second-mode squirming to first-mode squirming in (2.4), i.e. $\beta = B_2/B_1$. The values of the parameter β used here are from -5 to 10; the velocity field generated by a solitary squirmer with $\beta = 5$ is shown in figure 1 as an example, and those with $\beta = 1$ can be found in Ishikawa *et al.* (2006). When $|\beta| \leqslant 1$, there is

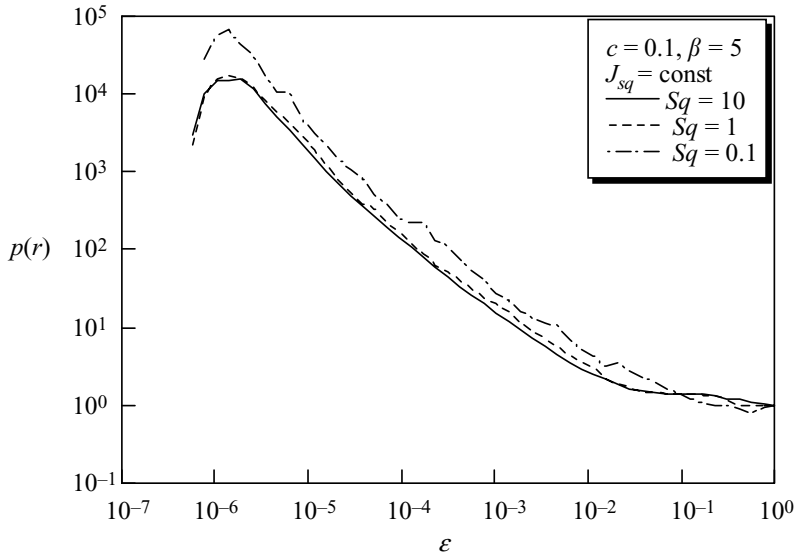

FIGURE 7. Normalized probability density function distribution for $Sq = 0.1$, 1 and 10 ($c = 0.1$ and $\beta = 5$). J_{sq} is kept constant, which corresponds to changing the ambient shear rate while the squirming velocity and the repulsive force between squirmers are kept constant.

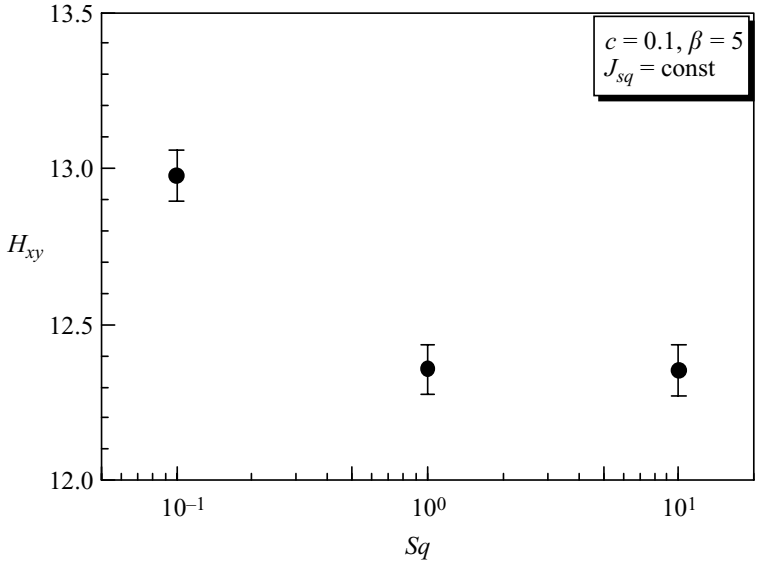

FIGURE 8. Particle stress component H_{xy} under the J_{sq} = const condition with $Sq = 0.1$, 1 and 10 ($c = 0.1$ and $\beta = 5$).

no recirculation region around the squirmer. The values $|\beta| = 5$ and 10 are chosen in order to observe in an obvious way the effect of second mode squirming. Recall that a squirmer with positive β is a *puller*, and that with negative β is a *pusher*. Thus the stresslet given by equation (1.4) is positive when β is positive, and negative when β is negative. The normalized probability densities with various β are shown in figure 9 ($c = 0.1$ and $Sq = 1$). (The result for inert spheres is shown in the figure as well). It is found that the minimum separation decreases with increasing $|\beta|$, and $p(r)$ with $\beta = 10$ has a small value in the near-field. The particle stress component H_{xy} in this case is shown in figure 10. (The result of the inert sphere case is shown as a broken line in the figure). We see that H_{xy} is smaller than that for inert spheres when β has positive values, but H_{xy} is not so much different from that of inert spheres when β

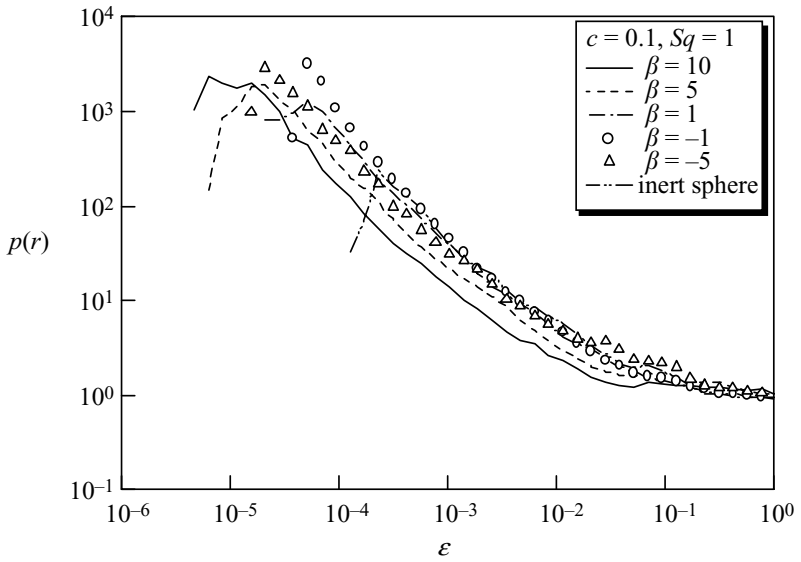

FIGURE 9. Normalized probability density function distribution for $\beta = 1$, 5 and 10 under the conditions of $c = 0.1$ and $Sq = 1$. The Result of the inert sphere case is also shown.

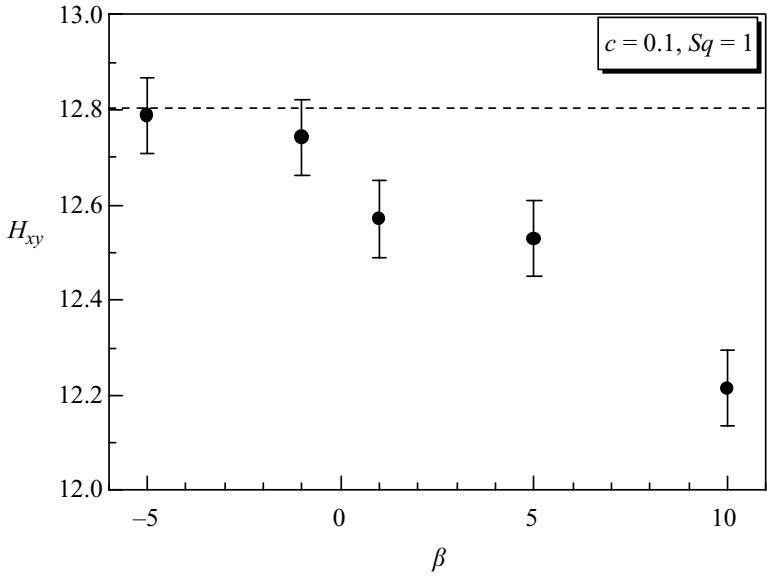

FIGURE 10. Particle stress component H_{xy} for $|\beta| = 1$, 5 and 10 under the conditions of $c = 0.1$ and $Sq = 1$. The result of the inert sphere case is shown as a broken line.

has negative values; however, increasing the second-mode squirming has the effect of reducing the apparent viscosity of the suspension slightly.

The apparent shear viscosity η in a dilute suspension of inert rigid spheres is given by

$$\eta = \mu \left(1 + \tfrac{5}{2}c + kc^2 + O(c^3)\right). \tag{3.4}$$

where the 5/2 was derived by Einstein (1906) and the constant k depends on the nature of the flow and on the magnitude of the Péclet number, defined as $Pe = Ua/D$. Here D is the self-diffusivity of particles, generated by Brownian motion (as in most of the studies reported in the literature) or by random or chaotic motion of different origins, as here. In the limit of strong Brownian motion ($Pe \ll 1$), Batchelor (1977) showed that k is the sum of a contribution k_1 due to purely hydrodynamic interactions (Batchelor quoted $k_1 = 5.2$, but it is now generally accepted that $k_1 = 5.0$;

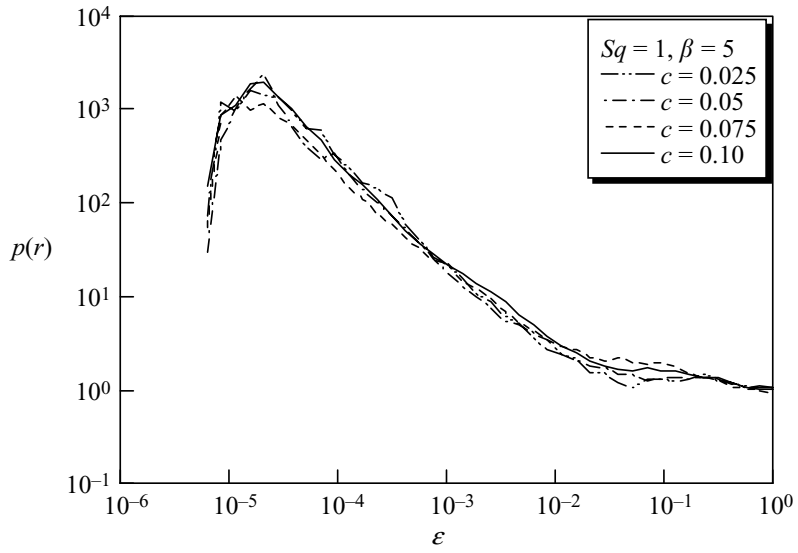

FIGURE 11. Normalized probability density function distribution for $c = 0.025, 0.05, 0.075$ and 0.1 under the conditions of $Sq = 1$ and $\beta = 5$.

(see Cichocki & Felderhof 1988), and another, $k_2 = 1.0$, directly attributable to the Brownian motion. In the limit of weak Brownian motion ($Pe \gg 1$), $k_2 = 0$, k_1 is still there, and there is another term, k_3, which comes from the effect on the configuration of the particles of the linear ambient flow. In the case of a pure straining motion, $k_3 = 2.4$ (Batchelor 1977), but for a simple shearing motion k_3 cannot be calculated because of the existence of closed particle orbits. The self-diffusivities of non-bottom-heavy squirmers are investigated by Ishikawa & Pedley (2007), and the results show that the Pe of squirmers with $\beta = 5$ is approximately $O(1)$, suggesting that there should not be any difficulty computing the effective viscosity even in simple shear.

The normalized probability densities in the present simulation with $c = 0.025$, 0.05, 0.075 and 0.1 are shown in figure 11 ($Sq = 1$ and $\beta = 5$). We see that the $p(r)$ distribution is not significantly affected by c. If $c \leqslant 0.1$ most of the interaction is pairwise and the particle distribution does not show large-scale micro-structure, so the normalized probability density should be similar. The apparent viscosity is, however, strongly dependent on c. The result is non-dimensionalized by μ and shown in figure 12 with equation (3.4). It is found that the apparent viscosity of the suspension of squirmers is very similar to that given by equation (3.4) with $k = 5.0$, i.e. for large Péclet number. The $O(c^2)$ term, as calculated for inert spheres by Batchelor & Green (1972*b*), is captured in the present simulation. The apparent viscosity of the suspension of squirmers is slightly smaller than that of inert spheres, but this is barely distinguishable in figure 12. (It is confirmed in Appendix B that our computations applied to inert spheres agree with equation (3.4), $k = 5.0$, for $c \leqslant 0.1$.) This result suggests that, notwithstanding the deterministic nature of our squirmers' trajectories, the overall effect of particle–particle interaction with squirming is *indistinguishable* from that with Brownian motion at these values of Sq and β.

4. A semi-dilute suspension of bottom-heavy squirmers

In the case of bottom-heavy squirmers there is an additional important parameter that is the direction of gravity relative to the background shear field. In this study the gravitational direction is taken successively in the $-\boldsymbol{x}$, $-\boldsymbol{y}$ and $-\boldsymbol{z}$ directions, while the background shear flow remains in the x,y-plane. The flow field is linear in

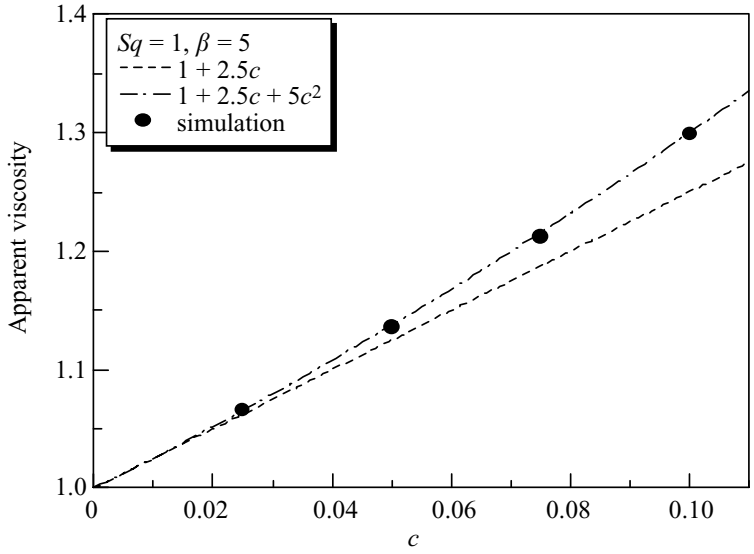

FIGURE 12. Change of the apparent viscosity of the suspension with c ($Sq = 1$ and $\beta = 5$). Einstein's analytical equation and Batchelor's analytical equation are also shown.

the Stokes flow regime; thus one can simply add two velocities in order to obtain the instantaneous velocities of bottom-heavy squirmers in a shear flow: (i) velocities of non-bottom-heavy squirmers in a shear flow, and (ii) velocities of bottom-heavy squirmers in a still fluid. The trajectories of squirmers, however, are not linear and one cannot simply add two trajectories in the same manner as the velocities. Other quantities such as the probability density and the suspension-averaged stress tensor also cannot be added in the same manner as the velocities. It is necessary to discuss separately the effect of bottom-heaviness in each gravitational direction relative to the background shear field.

G_{bh} is the ratio of the gravitational torque to a scale for the viscous torque, based on the squirming velocity, as defined by (2.11). If one assumes that the micro-organisms swim in water at 10 body lengths per second with their centre of mass $0.2a$ down from the geometric centre, G_{bh} is about 5 for micro-organisms with radius of 12.5 μm, and about 50 for micro-organisms with radius of 125 μm. The parameter range used in this section is $G_{bh} = 3$–100. The parameters for the repulsive force are $\alpha_1/(\mu a^2 \dot{\gamma}) = 10^{-2}$ and $\alpha_2 = 10^3$ throughout this section. The effect of the repulsive force is much smaller than the gravitational effect, so it will not be discussed in this section.

4.1. *Gravity is taken parallel to* $-\boldsymbol{x}$

In this case the shear flow is directed vertically, as in Kessler's (1986*a*) experiments using vertical pipe flow. The three-dimensional movement of 64 identical bottom-heavy squirmers in a simple shear flow field is computed for various G_{bh}. The other parameters are set as $c = 0.1$, $Sq = 1$ and $\beta = 5$. The velocity vectors of each squirmer relative to the background flow field are averaged over all squirmers in the computational cell during $t = 20 - 100$, and the results are shown in figure 13. We see that the length of the squirmer-averaged velocity vector increases with increasing G_{bh} and its direction approaches to the x-direction with increasing G_{bh}. This is because the more bottom-heavy the squirmers are, the more rapidly their swimming direction returns towards the vertical after an interaction; disturbances to this direction due to the background vorticity are also suppressed by the strong bottom-heaviness. Similar phenomena have been observed in experiments using real micro-organisms, such as

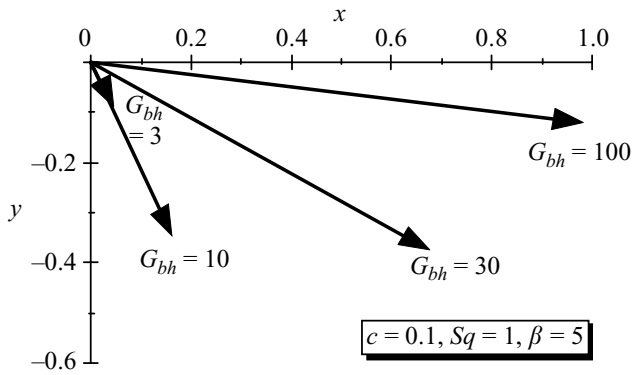

FIGURE 13. Squirmer-averaged velocity vectors relative to the background flow field with $G_{bh} = 3$, 10, 30 and 100 ($\boldsymbol{g}/g = -\boldsymbol{x}$, $c = 0.1$, $Sq = 1$ and $\beta = 5$).

Kessler's (1986*a*) pipe flow experiments. When the flow is directed downwards, the cells swim towards the pipe axis, forming a concentrated focused beam. When the flow is upwards, the cells swim towards its periphery, away from the fastest upflow. These tendencies are consistent with figure 13: the fact that the average velocity vector has a negative y-component means the squirmers are moving towards lower values of the upflow velocity. We will show squirmer-averaged velocity vectors under different conditions, and all of these results are consistent with the discussion in Pedley & Kessler (1992).

It may be helpful in understanding the squirmers' motion to introduce a normalized angular probability density function, defined as

$$p'(\theta_i) = \frac{2}{nV\sin(\theta_i)} \int\int_{\theta_i=\text{const}} P(\boldsymbol{r}, \boldsymbol{e})\, \mathrm{d}A_e\, \mathrm{d}V, \tag{4.1}$$

where $P(\boldsymbol{r}, \boldsymbol{e})\, \mathrm{d}A_e$ is the probability that there is a squirmer centred at $\boldsymbol{r}$ with orientation vector $\boldsymbol{e}$ within the solid angle $\mathrm{d}A_e$, and θ_i is the angle from the i-axis. $P(\boldsymbol{r}, \boldsymbol{e})$ satisfies the following equation:

$$\int\int P(\boldsymbol{r}, \boldsymbol{e})\, \mathrm{d}A_e\, \mathrm{d}V = N. \tag{4.2}$$

If one assumes isotropic orientation of squirmers, then $p'(\theta_i) = 1$ for all θ_i. The results for $p'(\theta_x)$ with various G_{bh} are shown in figure 14. When $G_{bh} = 3$ the $p'(\theta_x)$ distribution is almost isotropic, and the squirmers only gradually show a preferred direction as G_{bh} increases. Their average orientation vectors shift towards the x-axis with increasing G_{bh}, and the peak of $p'(\theta_x)$ increases with increasing G_{bh}. These results are consistent with the average velocity vectors shown in figure 13.

The stresslet of a solitary squirmer is given by (1.4), and it is a function of the orientation vector $\boldsymbol{e}$. The stresslet generated by a solitary squirmer has an order-c effect on the bulk stress, which is therefore strongly dependent on the squirmer orientations. The effect of G_{bh} on the particle stress component $H_{\boldsymbol{x}y}$ is shown in figure 15 ($c = 0.1$, $Sq = 1$ and $\beta = 5$). The symmetric part of H_{xy} is defined as $(H_{xy} + H_{yx})/2$, and the antisymmetric part of H_{xy} is defined as $(H_{xy} - H_{yx})/2$. In figure 15, we also show three kinds of contributions to the total stress: (i) the stress due to the background shearing motion (including the repulsive interactive force contribution), (ii) the stress due to the squirming motion, and (iii) the stress due to the bottom-heaviness. It is found that, as G_{bh} increases, the symmetric part becomes much lower than the inert sphere value of 12.8, and even negative for $30 \leqslant G_{bh} \leqslant 100$. The $G_{bh} = 30$ case shows

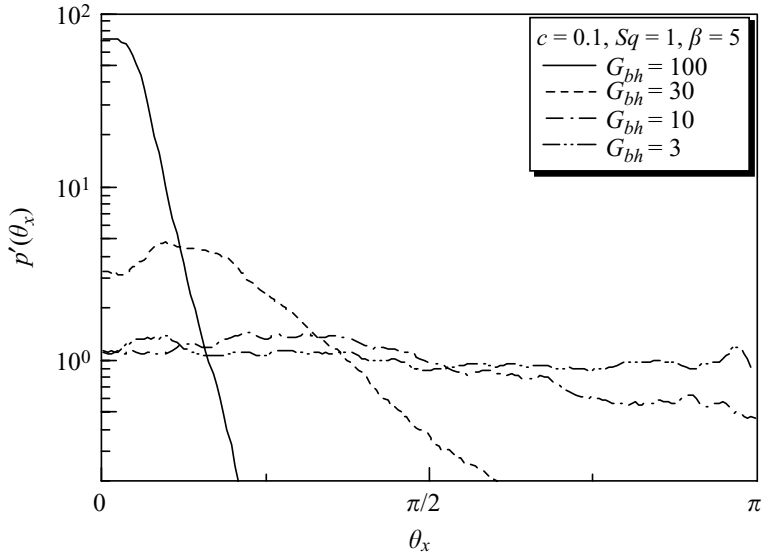

FIGURE 14. Normalized angular probability density distribution with $G_{bh} = 3$, 10, 30 and 100 ($\boldsymbol{g}/g = -\boldsymbol{x}$, $c = 0.1$, $Sq = 1$ and $\beta = 5$). (*a*) Symmetric part, (*b*) asymmetric part.

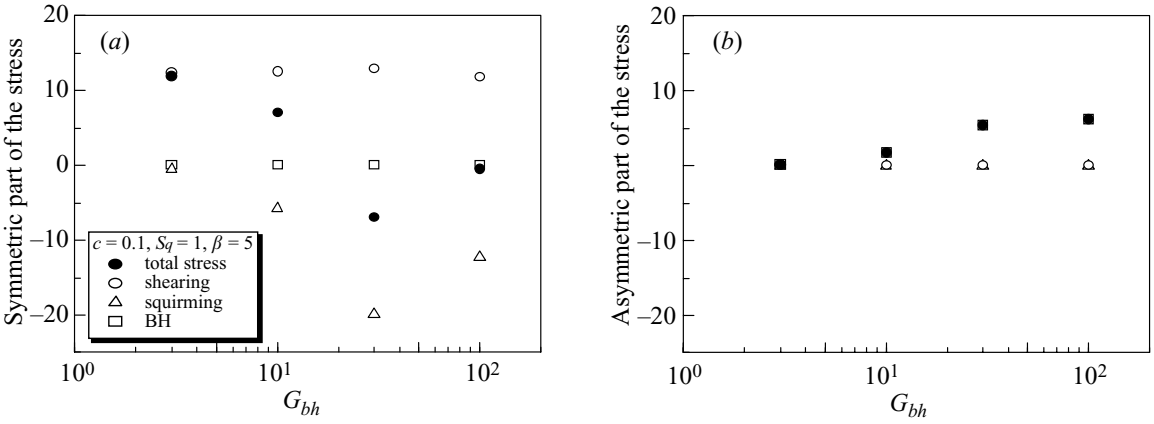

FIGURE 15. The effect of G_{bh} on the symmetric and asymmetric part of the particle stress components xy and yx ($\boldsymbol{g}/g = -\boldsymbol{x}$, $c = 0.1$, $Sq = 1$ and $\beta = 5$). 'Shearing' indicates the stress due to the shearing motion, 'squirming' indicates the stress due to the squirming motion, 'BH' indicates the stress due to the bottom-heaviness, and 'total stress' is the sum of these three. (*a*) First normal stress difference, (*b*) second normal stress difference.

the lowest value of the four cases shown, because it is at that value of G_{bh} that the squirming motions have their biggest effect. An antisymmetric part also appears in the case of bottom-heavy squirmers and it increases with increasing G_{bh}.

The effect of G_{bh} on H_{xy} looks complex; however, it can be explained by considering the orientation distributions shown in figures 13 and 14. If G_{bh} is so large that a solitary squirmer swims in the x-direction even in a shear flow, the (x,y)-component of the stresslet given by (1.4) is zero. If G_{bh} is so small that a solitary squirmer swims with the constant background vorticity, the (x,y)-component of the time-averaged stresslet is again zero because it is isotropic. The (x,y)-component of the stresslet for a solitary squirmer is negative when $e_x e_y$ is negative, and it has its minimum value when $\boldsymbol{e} = (\pm 1/\sqrt{2}, \mp 1/\sqrt{2}, 0)$, which corresponds to $\theta_x = \pi/4$. It is found from figure 13 that the squirmer-averaged velocity vectors are in the region $x > 0$, $y < 0$. This is why the symmetric part of H_{xy} becomes smaller than in the inert sphere case. We see from the $p'(\theta_x)$ distribution in figure 14 that the $G_{bh} = 30$ case has its large

peak around $\theta_x = \pi/8$. This is the reason why the symmetric part of H_{xy} is at its most negative then.

The asymmetric part of H_{xy} is generated by torques due to the bottom-heaviness. The rheological properties of a dilute suspension of dipolar spheres have been calculated by Brenner (1969), and the contribution of the torques due to bottom-heaviness to the (x,y)-component of the particle bulk stress $\Sigma_{xy}^{(p)}$ can be deduced to be

$$\left.\begin{aligned} \Sigma_{xy}^{(p)} &= \mu\dot{\gamma}\left(\tfrac{5}{2}c + \tfrac{3}{2}c\right), \quad G'_{bh} \geqslant 4\pi, \\ \Sigma_{xy}^{(p)} &= \mu\dot{\gamma}\left(\tfrac{5}{2}c\right), \qquad\quad 1 \gg G'_{bh}, \end{aligned}\right\} \tag{4.3}$$

where G'_{bh} is defined using $a\dot{\gamma}$ as a characteristic velocity in (2.11). In the case of a solitary inert sphere in a shear flow, the contribution of the bottom-heaviness does not exceed $1.5\,\mu\dot{\gamma}c$, which corresponds to 2π for dimensionless H_{xy}. In the case of a solitary squirmer, this result is still valid and the asymmetric part of H_{xy} again does not exceed 2π. However, in the case of two interacting squirmers, it can easily exceed 2π if Sq and G_{bh} are large enough. To simplify the explanation, let $Sq \gg 1$ and $G_{bh} \gg 1$, so that the background shear flow can be neglected. The torque exerted between two squirmers in near contact has been derived by Ishikawa *et al.* (2006), and the leading order in terms of ε is $\log(\varepsilon^{-1})$. As ε tends to zero, the torque due to the squirming motion increases as $\log(\varepsilon^{-1})$. This torque must be balanced against the external torque due to bottom-heaviness, because no rotational velocity will be generated under the $G_{\mathrm{bh}} \gg 1$ condition. As a result, the asymmetric part of H_{xy} increases as $\log(\varepsilon^{-1})$ when ε tends to zero. The hydrodynamic interactions between squirmers are not isotropic and are influenced by the gravitational direction relative to the background shear field; therefore they may increase or decrease the asymmetric part of time-averaged H_{xy}. In the case shown in figure 15, the asymmetric part of H_{xy} increases with G_{bh}. Consequently, this rheological effect for bottom-heavy squirmers is not due to cell–cell interactions, but due to the intrinsic stresslets on the aligned individual squirmers.

The stresslet of a solitary squirmer given by (1.4) contributes to normal stress differences as well. If the orientation vector of all (solitary) squirmers is in the x-direction, for instance, S_{xx} is equal to $-2S_{yy}$ and $-2S_{zz}$. The first normal stress difference, defined by $S_{xx} - S_{yy}$, is positive and the second normal stress difference, defined by $S_{yy} - S_{zz}$, is zero in this case. Thus the normal stress differences of the particle bulk stress are strongly dependent on the squirmer orientations. The effect of G_{bh} on normal stress differences of the particle stress is shown in figure 16 ($c = 0.1$, $Sq = 1$ and $\beta = 5$). The individual contributions to the total stress are shown as well. The first normal stress difference is defined as $H_{xx} - H_{yy}$, and the second normal stress difference is defined as $H_{yy} - H_{zz}$. When $G_{bh} = 3$, the normal stress differences are small. Because the $p'(\theta_x)$ distribution with $G_{bh} = 3$ is almost isotropic (see figure 14), the normal stress differences generated by individual squirmers cancel out overall. When $G_{bh} = 10$, the first normal stress difference is negative and the second normal stress difference is positive. This is because the squirmers in this case show a weakly preferred direction between $\theta_x = \pi/4$ and $\pi/2$ (see figure 14), and the first and second normal stress differences generated by a solitary squirmer with an orientation angle of $\pi/4 < \theta_x < \pi/2$ are negative and positive, respectively. When $G_{bh} = 100$, the first normal stress difference has a large positive value and the second normal stress difference becomes small. This tendency is similar to that expected for solitary squirmers swimming in the x-direction. The normal stress differences are strongly dependent on the squirmers' orientation, and their sign changes at $\theta_x = \pi/4$.

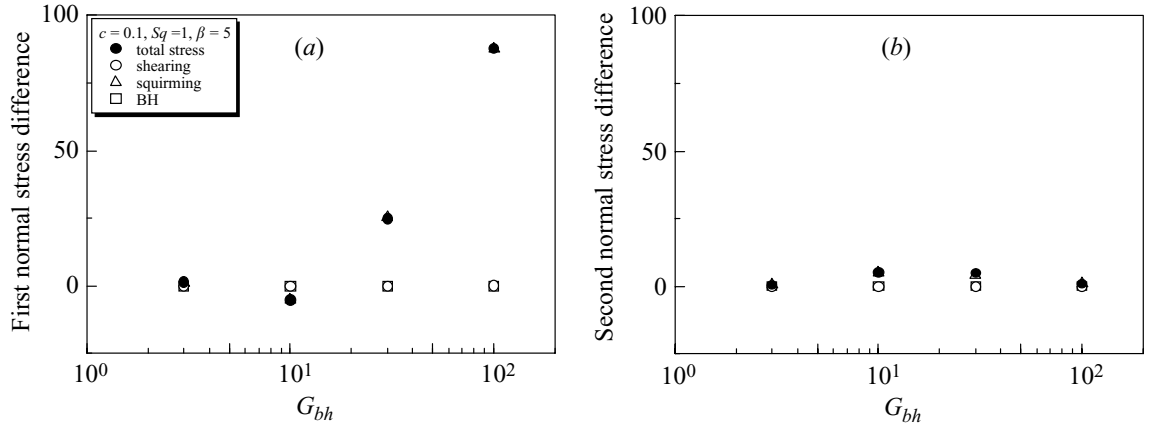

FIGURE 16. The effect of G_{bh} on the normal particle stress differences ($\boldsymbol{g}/g = -\boldsymbol{x}$, $c = 0.1$, $Sq = 1$ and $\beta = 5$). 'Shearing' indicates the stress due to the shearing motion, 'squirming' indicates the stress due to the squirming motion, 'BH' indicates the stress due to the bottom-heaviness, and 'total stress' is the sum of these three. (*a*) $G_{bh} = 10$, (*b*) $G_{bh} = 100$.

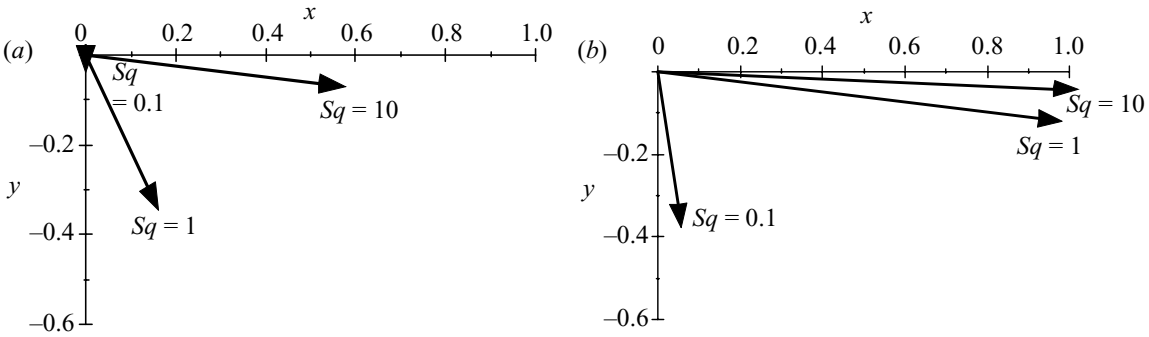

FIGURE 17. Squirmer-averaged velocity vectors relative to the background flow field under various *sq* conditions ($\boldsymbol{g}/g = -\boldsymbol{x}$, $c = 0.1$ and $\beta = 5$). The vectors are divided by *sq* in order to show all the vectors in the same figure. (*a*) $G_{bh} = 10$, (*b*) $G_{bh} = 100$.

Next the effect of Sq is investigated under the conditions of $c = 0.1$, $G_{bh} = 10$ and 100, and $\beta = 5$. The squirmer-averaged velocity vectors for $G_{bh} = 10$ and 100 are shown in figures 17(*a*) and 17(*b*), respectively. The dimensionless swimming velocity of a solitary squirmer is equal to Sq so the vectors in figure 17 are divided by Sq in order to show all the vectors in the same figure. We see that the squirmers tend to swim more in the x-direction as either G_{bh} or Sq is increased. The effect of G_{bh} is straightforward, and the effect of Sq may be explained as follows. Strong squirming motion induces strong interaction between squirmers, so the effect of the background vorticity of the shear flow decreases as Sq is increased. The effect of Sq on the particle stress component H_{xy} is shown in figure 18 ($c = 0.1$, $G_{bh} = 10$ and 100, and $\beta = 5$). It is found that the symmetric part decreases with increasing Sq and the antisymmetric part increases with increasing Sq. The symmetric result follows from the fact that when the gravitational direction is $-\boldsymbol{x}$, the squirming motion decreases the symmetric part of H_{xy}, as mentioned before, and the effect of squirming increases with increasing Sq. The asymmetric part of H_{xy} is much larger than 2π in the case of $G_{bh} = 100$ and $Sq = 10$. This is because the effect of the background shear flow is small when $Sq = 10$, and the torque due to the squirming motion of two squirmers has to be balanced with the external torque. Since the torque generated by two squirmers in near contact increases as $\log(\varepsilon^{-1})$ when ε tends to zero, the asymmetric part of H_{xy} may also become larger than 2π.

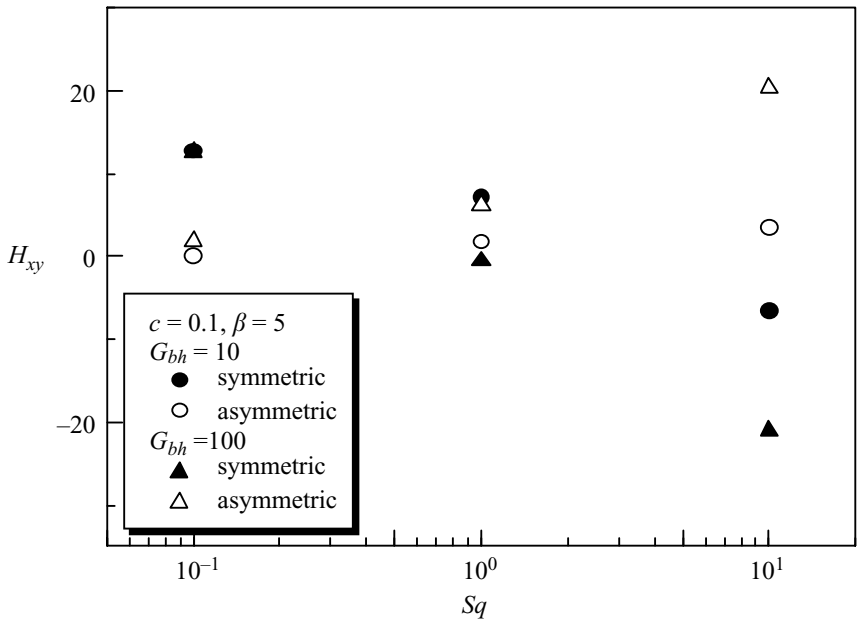

FIGURE 18. The effect of Sq on the particle stress component H_{xy} ($\boldsymbol{g}/g = -\boldsymbol{x}$, $c = 0.1$, $G_{bh} = 10$ and 100, and $\beta = 5$). H_{xy} is split into symmetric and antisymmetric parts which are shown separately.

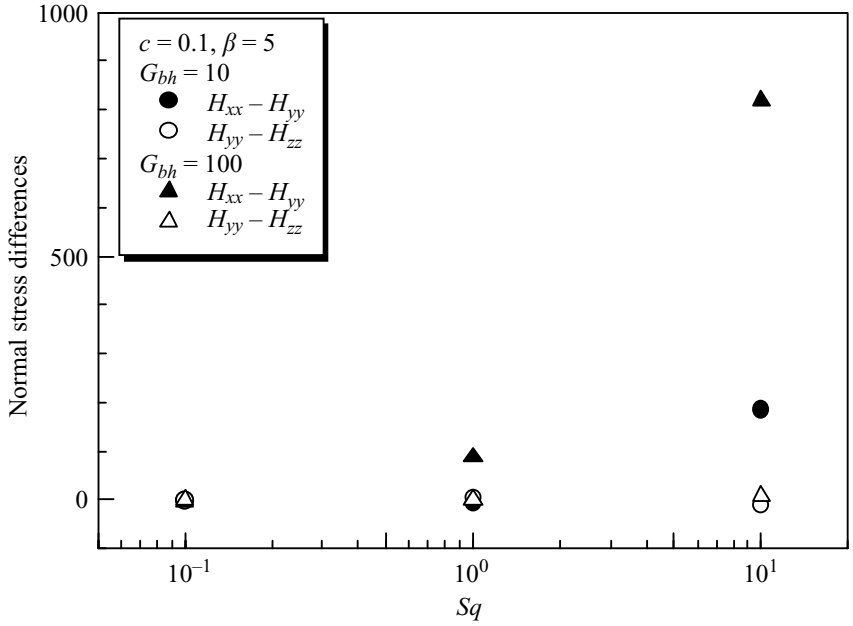

FIGURE 19. The effect of Sq on the normal particle stress differences ($\boldsymbol{g}/g = -\boldsymbol{x}$, $c = 0.1$, $G_{bh} = 10$ and 100, and $\beta = 5$). (*a*) $G_{bh} = 10$, (*b*) $G_{bh} = 100$.

The effect of Sq on the normal stress differences is shown in figure 19 ($c = 0.1$, $G_{bh} = 10$ and 100, and $\beta = 5$). We see that the first normal stress difference increases with increasing Sq. This is because the first normal stress difference for solitary squirmers swimming in the x-direction is proportional to the second squirming mode B_2 as given by (1.4), and hence is proportional to the parameter Sq.

The effect of β is investigated under the conditions of $c = 0.1$, $Sq = 1$, $G_{bh} = 10$ and 100. In the case of two interacting squirmers (Ishikawa *et al.* 2006), the absolute value of β has the effect of enhancing the interaction between squirmers and they change their orientations at greater separation distances as $|\beta|$ is increased. The

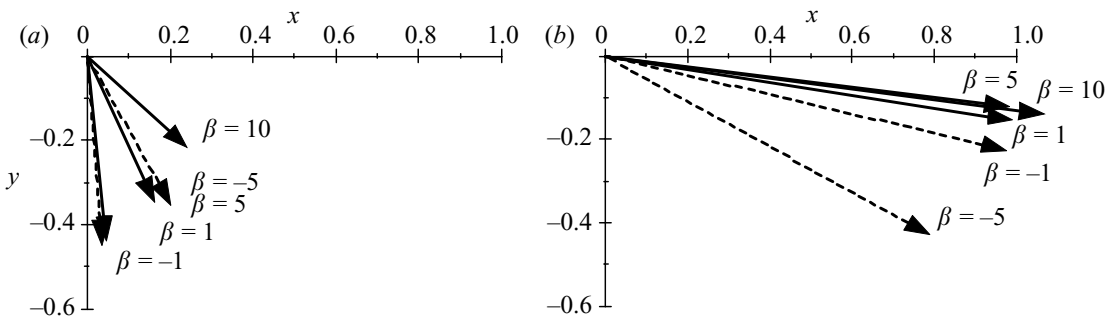

FIGURE 20. Squirmer-averaged velocity vectors relative to the background flow field under various β conditions ($\boldsymbol{g}/g = -\boldsymbol{x}$, $c = 0.1$ and $Sq = 1$). (*a*) $G_{bh} = 10$, (*b*) $G_{bh} = 100$.

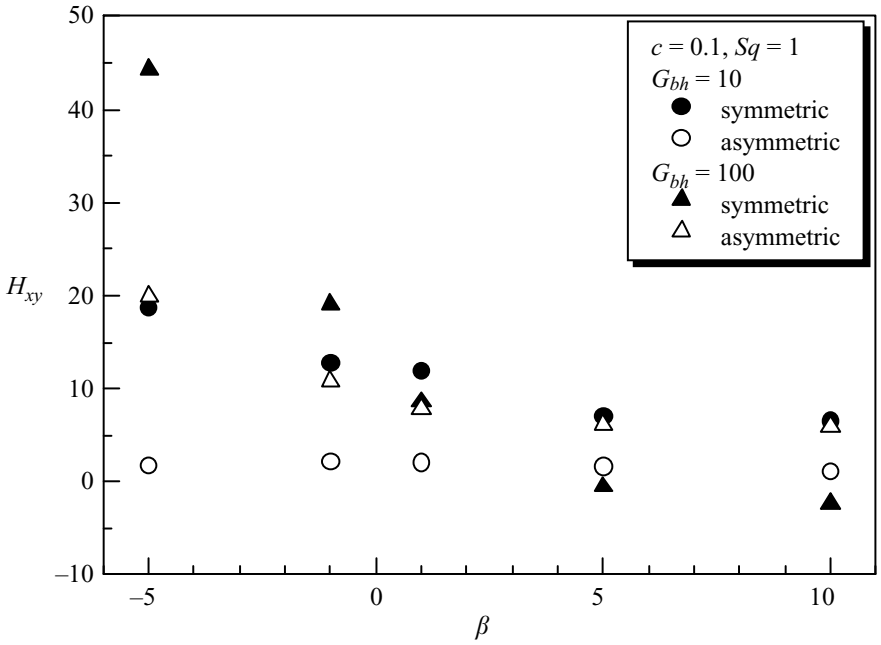

FIGURE 21. The effect of β on the particle stress component H_{xy} ($\boldsymbol{g}/g = -\boldsymbol{x}$, $c = 0.1$, $Sq = 1$, and $G_{bh} = 10$ and 100). H_{xy} is split into symmetric and antisymmetric parts which are shown separately.

squirmer-averaged velocity vectors for $G_{bh} = 10$ and 100 are shown in figures 20(*a*) and 20(*b*), respectively, where the results with negative β are drawn as broken lines. For $G_{bh} = 10$, there is a tendency for the squirmers to swim increasingly in the x-direction as $|\beta|$ is increased. This is because the disturbance due to hydrodynamic interaction increases as $|\beta|$ is increased, so the effect of the background vorticity decreases compared with the hydrodynamic interaction. This is presumably the reason why the averaged velocity vector comes closer to the x-axis, though the vector length decreases, for large $|\beta|$. In the case of $G_{bh} = 100$, the effect of β appears especially when $\beta = -5$. Under large G_{bh} conditions, squirmers tend to swim upward. Two squirmers with positive β attract each other when they are aligned vertically, whereas two squirmers with negative β repel each other. Thus two squirmers with negative β interact when they are further apart than those with positive β, which may be the reason why the orientation vector of squirmers with $\beta = -5$ is shifted from the x-direction.

The effect of β on the particle stress component H_{xy} is shown in figure 21 ($c = 0.1$, $Sq = 1$ and $G_{bh} = 10$ and 100). The stresslet S_{xy} for a solitary squirmer is positive when β is negative, but negative when β is positive, if the orientation vector satisfies $e_x e_y < 0$.

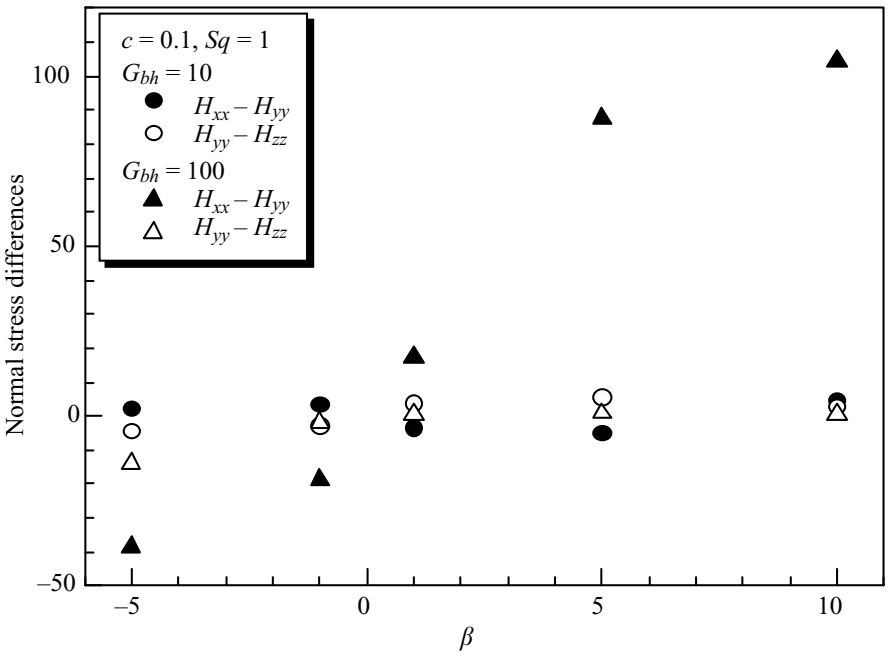

FIGURE 22. The effect of β on the normal particle stress differences ($\boldsymbol{g}/g = -\boldsymbol{x}$, $c = 0.1$, $Sq = 1$, and $G_{bh} = 10$ and 100). (*a*) $G_{bh} = 10$, (*b*) $G_{bh} = 100$.

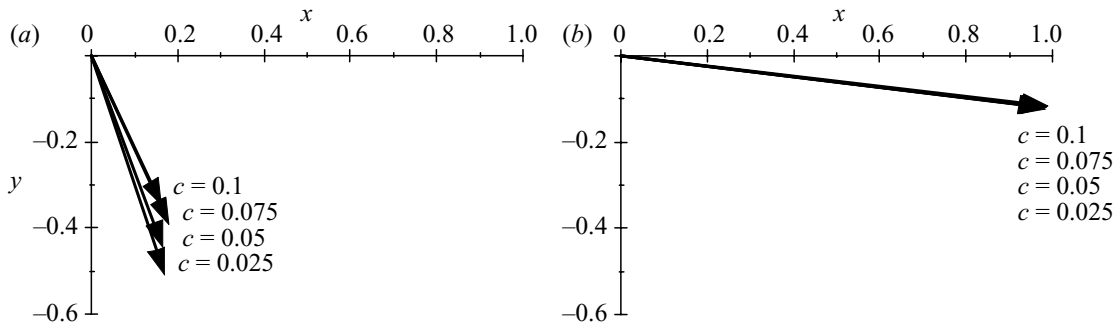

FIGURE 23. Squirmer-averaged velocity vectors relative to the background flow field under various c conditions ($\boldsymbol{g}/g = -\boldsymbol{x}$, $Sq = 1$ and $\beta = 5$). (*a*) $G_{bh} = 10$, (*b*) $G_{bh} = 100$.

Since the symmetric part is directly influenced by the stresslet due to squirming, it decreases with increasing β. The effect of β on the normal stress differences is shown in figure 22 ($c = 0.1$, $Sq = 1$ and $G_{bh} = 10$ and 100). We see that a large first normal stress difference appears in the case of $G_{bh} = 100$ and a negative first normal stress difference appears when β is negative. This is because the first normal stress difference for a solitary squirmer is proportional to β, as given by (1.4), and changes its sign with β. We can say, therefore, the sign and the strength of normal stress differences are strongly dependent on β.

Lastly, the effect of c is investigated under the conditions of $Sq = 1$, $G_{bh} = 10$ and 100, and $\beta = 5$. The squirmer-averaged velocity vectors for $G_{bh} = 10$ and 100 are shown in figures 23(*a*) and 23(*b*), respectively. In the case of $G_{bh} = 10$, the length of the velocity vectors decreases as c is increased. The disturbance due to hydrodynamic interaction increases with increasing c, so the orientations of the velocity vectors are more widely dispersed for larger c, which results in the shortening of the squirmer-averaged velocity vectors. In the case of $G_{bh} = 100$, the effect of c is not significant, because, again, the effect of the bottom-heaviness is too large for the hydrodynamic interaction to be important.

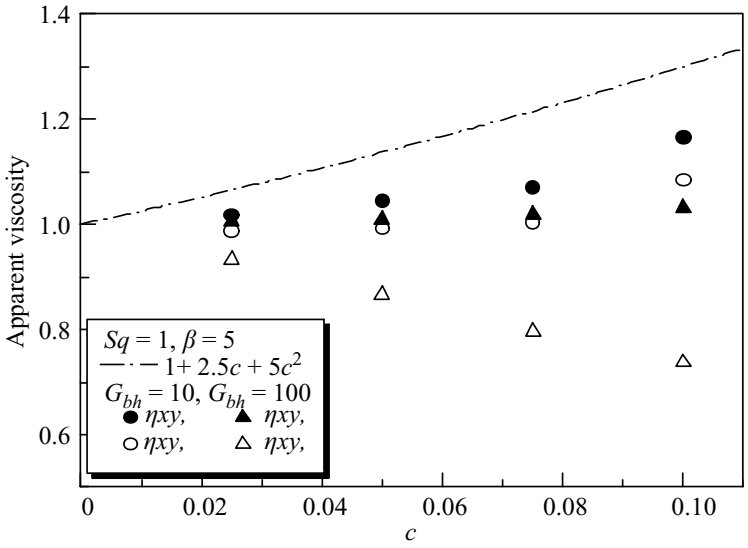

FIGURE 24. Change of the apparent viscosity of the suspension with c ($\boldsymbol{g}/g = -\boldsymbol{x}$, $Sq = 1$, $\beta = 5$ and $G_{bh} = 10$ and 100). Two kinds of apparent viscosities are shown as well as Batchelor's analytical equation.

The rheology of a suspension is often discussed in terms of an apparent viscosity and of normal stress difference coefficients. The apparent viscosity of the suspension of non-bottom-heavy squirmers can be calculated from (3.2), but this is not appropriate in the case of bottom-heavy squirmers. A suspension of bottom-heavy squirmers shows non-Newtonian properties, and H_{xy} is not equal to H_{yx}. Therefore, we will introduce two types of apparent viscosity η_{xy} and η_{yx} as

$$\eta_{xy} = \mu\left(1 + \frac{3}{4\pi}\frac{H_{xy}}{\mu\dot{\gamma}}c\right), \quad \eta_{yx} = \mu\left(1 + \frac{3}{4\pi}\frac{H_{yx}}{\mu\dot{\gamma}}c\right). \tag{4.4}$$

(If one defines the apparent viscosity by using the symmetric part of H_{xy}, then it corresponds to $(\eta_{xy} + \eta_{yx})/2$.) The first and second normal stress difference coefficients are calculated as

$$\phi_1 = \frac{3\mu}{4\pi\dot{\gamma}^2}(H_{xx} - H_{yy})c, \quad \phi_2 = \frac{3\mu}{4\pi\dot{\gamma}^2}(H_{yy} - H_{zz})c. \tag{4.5}$$

The effect of c on the apparent viscosities, which are non-dimensionalized by dividing by μ, is shown in figure 24 under the conditions of $Sq = 1$, $G_{bh} = 10$ and 100, and $\beta = 5$. The equation (3.4) with $k = 0.5$ is shown in the figure as well. It is found that all apparent viscosities are lower than given by this equation, and the difference increases with increasing G_{bh} and c. Under the condition that gravity acts in the $-\boldsymbol{x}$-direction, the apparent viscosity of the suspension of bottom-heavy squirmers is smaller than that of a suspension of inert spheres. Moreover, it can even become smaller than the viscosity of the solvent fluid. The bulk stress of a suspension is given by (1.1), and the apparent viscosity of the suspension is smaller than the viscosity of the solvent fluid when the particle stress is negative. The particle stress can be calculated from the stresslet of individual particles given by (1.2). The stresslet of a solitary squirmer in a shear flow is the sum of the stresslet due to the background shear flow and that due to the squirming motion, where the effect of the bottom-heaviness is omitted for simplicity. The xy-component of the stresslet due to squirming becomes negative when $e_x e_y$ is negative, as given by (1.4). Therefore, the particle stress can be negative

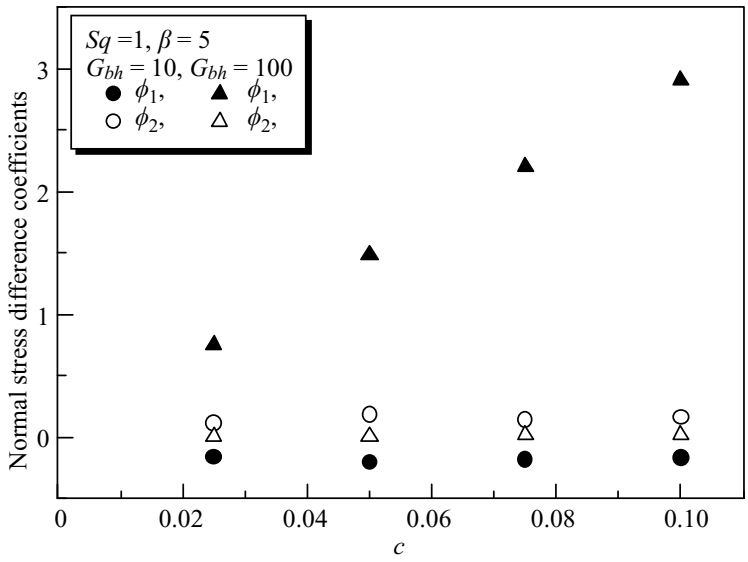

FIGURE 25. Change of the normal stress difference coefficients with c ($\boldsymbol{g}/g = -\boldsymbol{x}$, $Sq = 1$, $\beta = 5$ and $G_{bh} = 10$ and 100).

if the squirming motion is strong compared with the background shear flow and the orientation vector of the squirmer is in the $x > 0$, $y < 0$ quadrant.

The effect of c on the normal stress difference coefficients, which are non-dimensionalized by using $\mu/\dot{\gamma}$, are shown in figure 25. It is found that the suspension of bottom-heavy squirmers shows considerable normal stress differences. The sign and the strength of normal stress differences are dependent on the orientation of squirmers, so they are influenced mainly by the gravitational direction, G_{bh} and sign of β. The rheological effect for bottom-heavy squirmers is, therefore, mainly due to the intrinsic stresslets on the aligned individual squirmers in a semi-dilute regime.

4.2. *Gravity is taken parallel to* $-\boldsymbol{y}$

In this section gravity is taken in the $-\boldsymbol{y}$-direction and the three-dimensional motion of 64 identical bottom-heavy squirmers is again computed in a simple shear flow field, which is now horizontal and varies with the vertical coordinate. The results for the particle bulk stress are completely different from those of § 4.1.

Firstly the effect of G_{bh} on the orientation of squirmers is shown in figure 26 in terms of the normalized angular probability density $p'(\theta_y)$ defined by (4.1). When $G_{bh} = 3$ the $p'(\theta_y)$ distribution is almost isotropic, but again, as G_{bh} is increased, the squirmers increasingly show a preferred direction. Their average orientation vectors shift towards the y-axis as G_{bh} is increased, and the peak of $p'(\theta_y)$ increases. These tendencies are quite similar to those shown in figure 14.

The effect of G_{bh} on the particle stress component H_{xy} is shown in figure 27 ($c = 0.1$, $Sq = 1$ and $\beta = 5$), in which we also show three kinds of contributions to the total stress: (i) the stress due to the background shearing motion (including the repulsive interactive force contribution), (ii) the stress due to the squirming motion, and (iii) the stress due to the bottom-heaviness. We see that the symmetric part becomes much larger than the inert sphere value of 12.8, and the $G_{bh} = 30$ case shows the largest value of the four cases computed. These results are almost the opposite of the results of figure 15, for which the gravitational direction was parallel to $-\boldsymbol{x}$. This can be explained by considering the orientation distributions shown in figure 26. If G_{bh} is so large that a solitary squirmer swims in the y-direction, the (x,y)-component of the stresslet given by (1.4) is zero. However, H_{xy} should be large because the squirmer

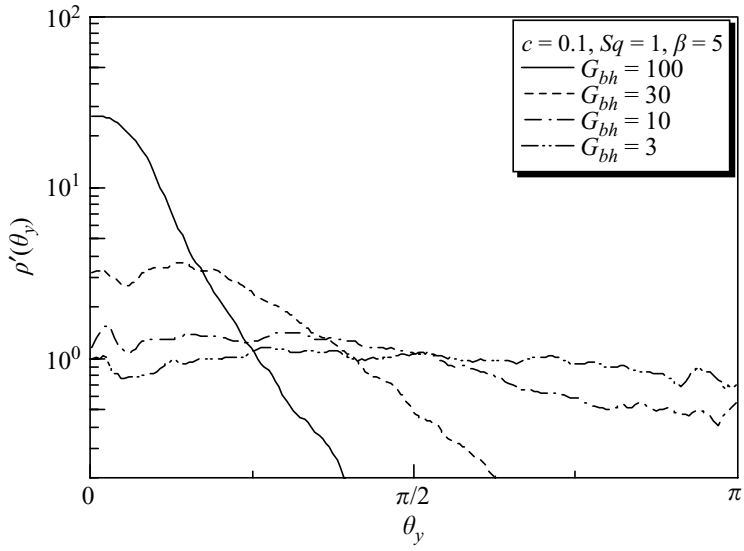

FIGURE 26. Normalized angular probability density distribution with $G_{bh} = 3$, 10, 30 and 100 ($\boldsymbol{g}/g = -\boldsymbol{y}$, $c = 0.1$, $Sq = 1$ and $\beta = 5$). (*a*) Symmetric part, (*b*) asymmetric part.

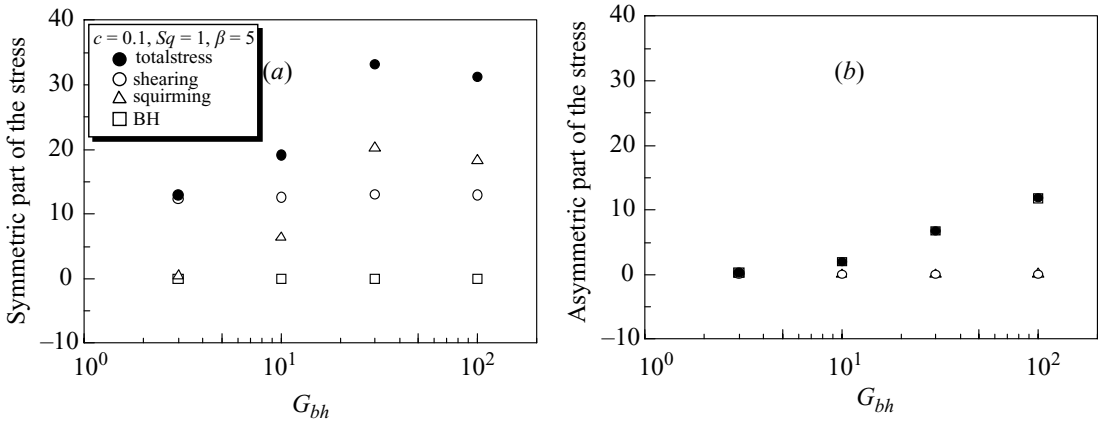

FIGURE 27. The effect of G_{bh} on the symmetric and asymmetric part of the particle stress components xy and yx ($\boldsymbol{g}/g = -\boldsymbol{y}$, $c = 0.1$, $Sq = 1$ and $\beta = 5$). 'Shearing' indicates the stress due to the shearing motion, 'squirming' indicates the stress due to the squirming motion, 'BH' indicates the stress due to the bottom-heaviness, and 'total stress' is the sum of these three. (*a*) First normal stress difference, (*b*) second normal stress difference.

swims across the shear. If G_{bh} is so small that a solitary squirmer swims with the constant background vorticity, the (x,y)-component of the time-averaged stresslet is zero because the squirmer stresslet is isotropic. The (x,y)-component of the stresslet given by (1.4) is positive when $e_x e_y$ is positive, and it has its maximum value when $\boldsymbol{e} = (\pm 1/\sqrt{2}, \pm 1/\sqrt{2}, 0)$, which corresponds to $\theta_y = \pi/4$. If the squirmer swims across the shear, the H_{xy} becomes larger than the stresslet given by (1.4). Consequently, the $\pi/2$ radian rotation of the gravitational direction in the x,y-plane induces almost the opposite effect of squirming on the symmetric part of H_{xy}. The asymmetric part increases with increasing G_{bh}, and this tendency is the same as in figure 15. This is because the asymmetric part is generated by the torques due to the bottom-heaviness, and the direction of the squirmer-averaged torque does not change even though the gravitational direction is changed in the x,y-plane, provided that the background vorticity is invariant.

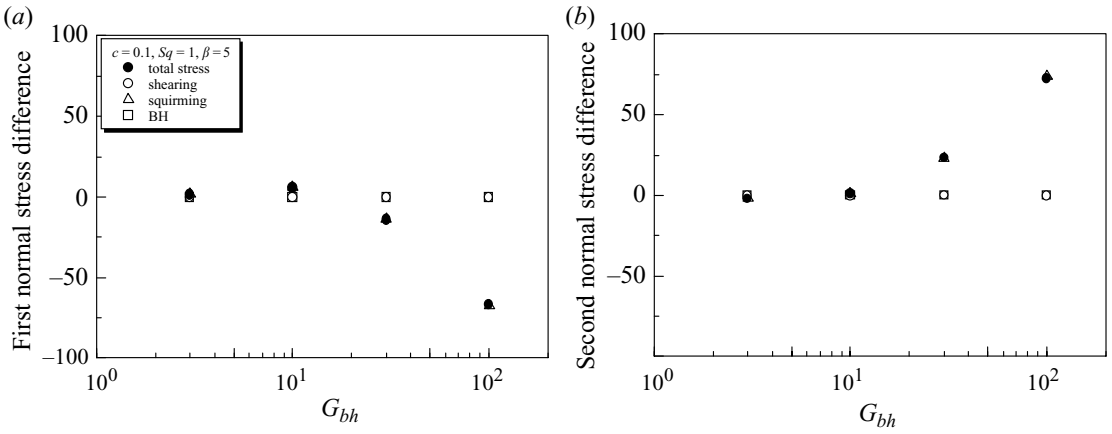

FIGURE 28. The effect of G_{bh} on the normal particle stress differences ($\boldsymbol{g}/g = -\boldsymbol{y}$, $c = 0.1$, $Sq = 1$ and $\beta = 5$). Where 'Shearing' indicates the stress due to the shearing motion, 'squirming' indicates the stress due to the squirming motion, 'BH' indicates the stress due to the bottom-heaviness, and 'total stress' is the sum of these three.

The effect of G_{bh} on normal stress differences is shown in figure 28 ($c = 0.1$, $Sq = 1$ and $\beta = 5$) The individual contributions to the total stress are shown as well. It is found that the first normal stress difference is negative and the second normal stress difference is positive when G_{bh} is large. These tendencies are also different from those shown in figure 16, in which the first normal stress difference is positive and the second normal stress difference is almost zero when G_{bh} is large. This can be explained as follows. If the orientation vector of a solitary squirmer is in the y-direction, S_{yy} is equal to $-2S_{xx}$ and $-2S_{zz}$ as given by (1.4). The first normal stress difference defined by $S_{xx} - S_{yy}$, in this case, is negative and the second normal stress difference defined by $S_{yy} - S_{zz}$ is positive. The dominant normal stress in this case is S_{yy} instead of S_{xx}. Thus both normal stresses of the particle bulk stress are generated, but with opposite sign. Consequently, the $\pi/2$ radian rotation of the gravitational direction from the x-axis induces the opposite effect of squirming on the first normal stress difference and has the new effect of generating a large second normal stress difference. Thus the rheological effect for bottom-heavy squirmers is again explained by the intrinsic stresslets on the aligned individual squirmers.

Next the effect of Sq on the particle stress component H_{xy} is shown in figure 29 ($c = 0.1$, $G_{bh} = 10$ and 100, and $\beta = 5$). Since the gravitational direction is $-\boldsymbol{y}$, the squirming motion has the effect of increasing the symmetric part of H_{xy}. Since the effect of squirming increases with increasing Sq, the symmetric part also increases with Sq. In addition, we see that the asymmetric part of H_{xy} increases with increasing Sq as well, which is a similar tendency to that in figure 18. The effect of Sq on normal stress differences is shown in figure 30 ($c = 0.1$, $G_{bh} = 10$ and 100, and $\beta = 5$). It is found that the absolute values of both normal stress differences increase with increasing Sq. A similar tendency was found in figure 19, though the sign of the first normal stress difference is opposite and the second normal stress difference is newly generated in this case.

The effect of β on the particle stress component H_{xy} is shown in figure 31 ($c = 0.1$, $Sq = 1$ and $G_{bh} = 10$ and 100). We see that the symmetric part increases with increasing β, because the stresslet for a solitary squirmer is proportional to the second mode squirming as given by (1.4). The asymmetric part is not significantly influenced by β in this case. The effect of β on normal stress differences is shown in figure 32 ($c = 0.1$, $Sq = 1$ and $G_{bh} = 10$ and 100). It is found that large normal stress differences

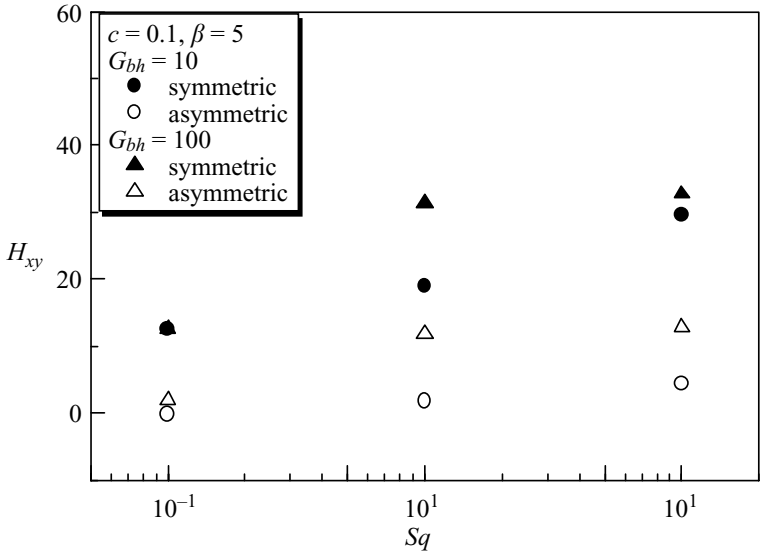

FIGURE 29. The effect of Sq on the particle stress component H_{xy} ($\boldsymbol{g}/g = -\boldsymbol{y}$, $c = 0.1$, $G_{bh} = 10$ and 100, and $\beta = 5$). H_{xy} is split into symmetric and antisymmetric parts which are shown separately.

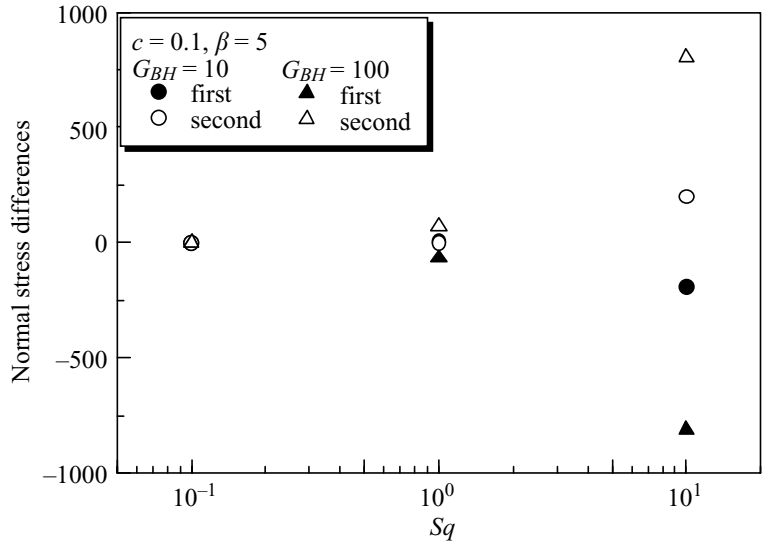

FIGURE 30. The effect of Sq on the normal particle stress differences ($\boldsymbol{g}/g = -\boldsymbol{y}$, $c = 0.1$, $G_{bh} = 10$ and 100, and $\beta = 5$).

appear in the case of $G_{bh} = 100$ and their absolute values increase with increasing β: This is because the stresslet due to squirming increases with $|\beta|$ as given by (1.4). Basically β and Sq enhance the squirming effect on the particle bulk stress, whatever the gravitational direction and G_{bh}. The main properties of the particle bulk stress, such as the sign of its components, are principally dominated by the gravitational direction, G_{bh} and sign of β.

Lastly the effect of c on the dimensionless apparent viscosities, defined by (4.4), is shown in figure 33 under the conditions of $Sq = 1$, $G_{bh} = 10$ and 100, and $\beta = 5$. The equation (3.4) with $k = 5.0$ is shown in the figure as well. It is found that all apparent viscosities are larger than given by equation (3.4) with $k = 5.0$, and the difference increases with increasing G_{bh} and c. For a horizontal shear flow, the apparent viscosity of the suspension of bottom-heavy squirmers is larger than that of a suspension of inert spheres. This result is completely different from that shown in figure 24 for a

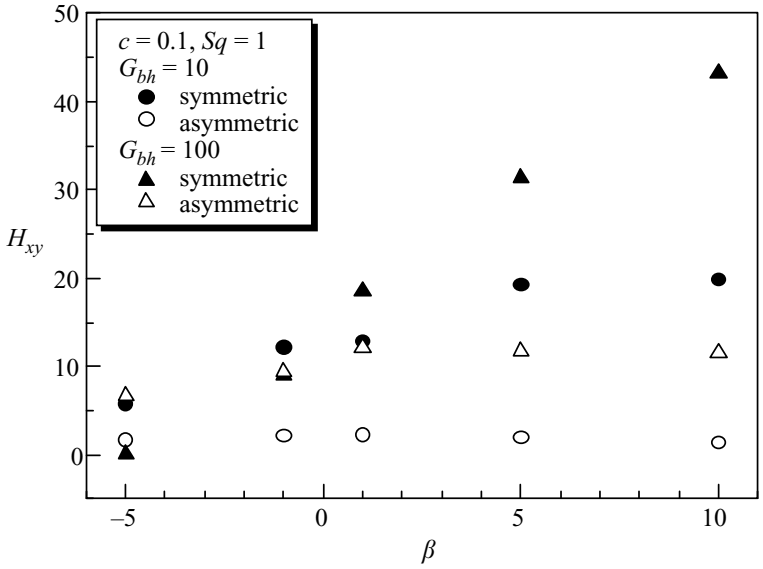

FIGURE 31. The effect of β on the particle stress component H_{xy} ($\boldsymbol{g}/g = -\boldsymbol{y}$, $c = 0.1$, $Sq = 1$, and $G_{bh} = 10$ and 100). H_{xy} is split into symmetric and antisymmetric parts which are shown separately.

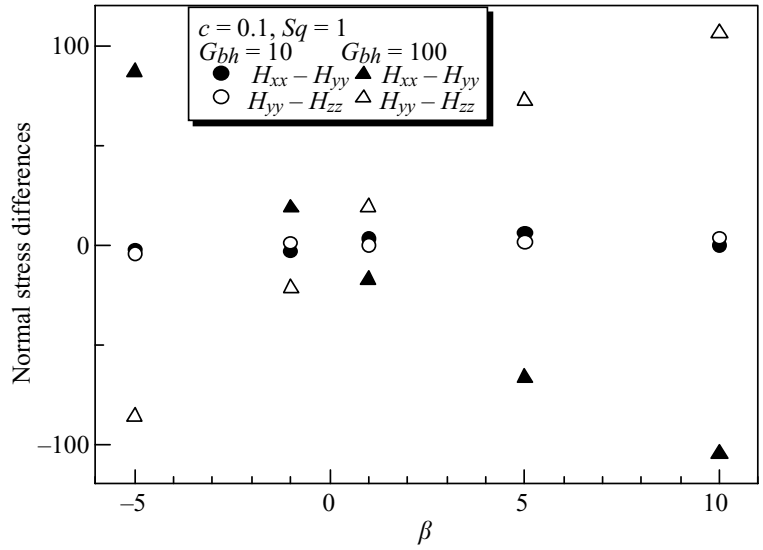

FIGURE 32. The effect of β on the normal particle stress differences ($\boldsymbol{g}/g = -\boldsymbol{y}$, $c = 0.1$, $Sq = 1$, and $G_{bh} = 10$ and 100).

vertical shear flow. It follows from the tendency of the squirmers to swim upwards, across the shear flow streamlines. The effect of c on the dimensionless normal stress difference coefficients, which are defined by (4.5), are shown in figure 34. It is found that a suspension of bottom-heavy squirmers shows considerable first and second normal stress differences. The first normal stress difference coefficient is opposite in sign to the results shown in figure 25, and the large second normal stress difference is generated in this case. The rheology of a suspension of bottom-heavy squirmers is, therefore, strongly influenced by the gravitational direction, G_{bh} and sign of β.

4.3. *Gravity is taken parallel to* $-z$

When gravity is taken in the $-z$-direction, so that the shear flow is horizontal and does not vary with the vertical coordinate, the effect of squirming on the rheology of the suspension is rather small compared with the cases already considered. Assuming

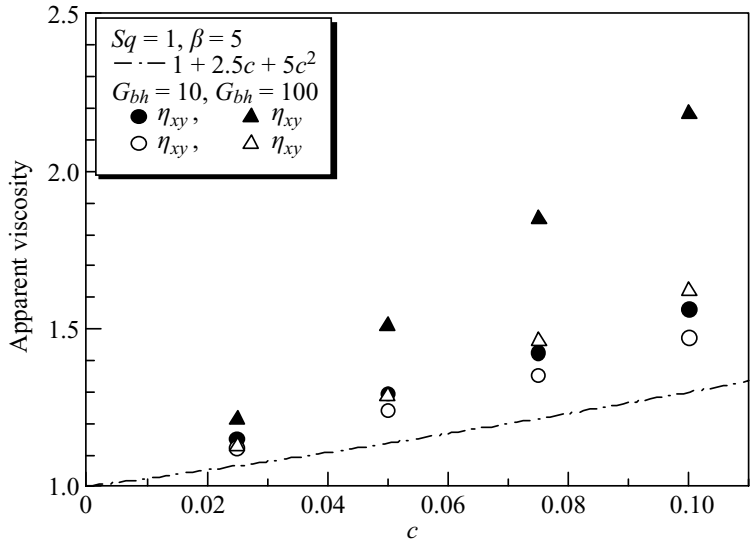

FIGURE 33. Change of the apparent viscosity of the suspension with c ($\boldsymbol{g}/g = -\boldsymbol{y}$, $Sq = 1$, $\beta = 5$ and $G_{bh} = 10$ and 100). Two kinds of apparent viscosities are shown as well as Batchelor's analytical equation.

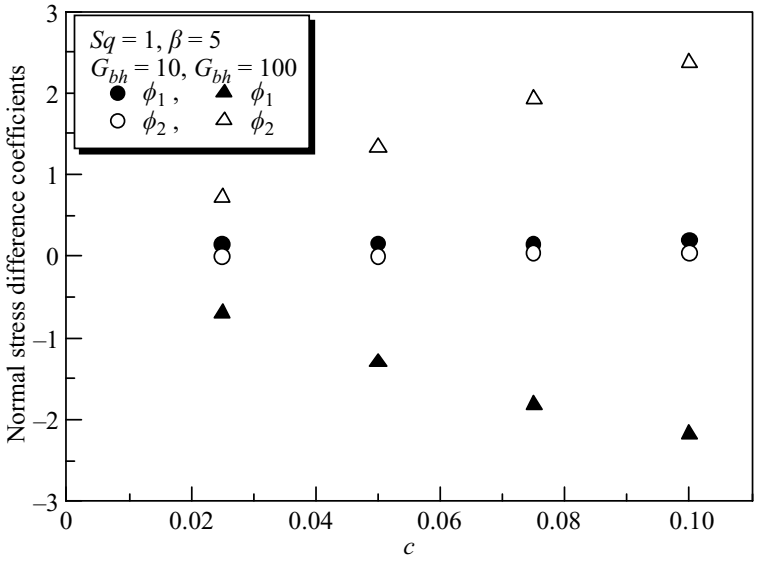

FIGURE 34. Change of the normal stress difference coefficients with c ($\boldsymbol{g}/g = -\boldsymbol{y}$, $Sq = 1$, $\beta = 5$ and $G_{bh} = 10$ and 100).

a solitary squirmer oriented in the z-direction, the stresslet due to the squirming motion satisfies $S_{xy} = S_{yz} = 0$ and $S_{zz} = -2S_{xx} = -2S_{yy}$ as given by (1.4). Therefore, the apparent viscosity of a dilute suspension of those squirmers is equal to that of inert spheres in this case. The first normal stress difference of the dilute suspension of the squirmers is zero, which is again the same as in the inert sphere case. However, there is one major difference: the second normal stress difference, which does appear, and its strength can be calculated from (1.4).

In the case of a semi-dilute suspension, the orientation vectors of squirmers are not exactly parallel to the z-axis because of the hydrodynamic interaction. The effect of G_{bh} on the orientation of squirmers is shown in figure 35, where the normalized angular probability density $p'(\theta_z)$ defined by (4.1) is plotted. The results for bottom-heavy inert spheres, which corresponds to $Sq = 0$, are shown in the figure as well (G'_{bh} is defined using $a\dot{\gamma}$ as a characteristic velocity in (2.11)). It is found that the angular

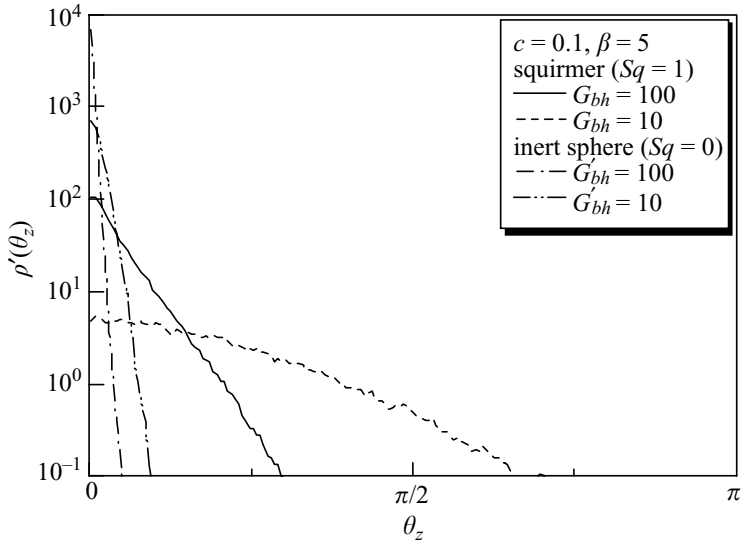

FIGURE 35. Normalized angular probability density distribution for squirmers and inert spheres under the condition of $\boldsymbol{g}/g = -\boldsymbol{z}$. The other parameters are $c = 0.1$, G_{bh} or $G'_{bh} = 10$ and 100, $Sq = 1$ or 0, and $\beta = 5$.

probability has its maximum value at $\theta_z = 0$ in all cases, which means the squirmers and spheres are swimming or are orientated in the z-direction on average. The peak in the figure is decreased by the hydrodynamic interaction due to the squirming motion, but there is no deviation of the peak from the z-axis. When the orientation vectors are in the z-direction on average, the former discussion about a solitary squirmer orientated in the z-direction is still useful for a rough estimate of the suspension rheology. The results are straightforward, and are therefore omitted from this paper.

5. Summary and discussion

In this paper a micro-organism is modelled as a squirming sphere with prescribed tangential surface velocity, in which the centre of mass of the sphere may be displaced from the geometric centre (bottom-heaviness). The effects of inertia and Brownian motion are neglected. The three-dimensional motion of 64 identical squirmers in a simple shear flow field, and contained in a cube with periodic boundary conditions, is computed, and the rheological properties of a semi-dilute suspension of squirmers are investigated.

Whether or not a squirmer has bottom-heaviness generates essential differences in the rheology. In the case of *non-bottom-heavy* squirmers, the stresslet generated by the squirming motion is isotropic and there is no direct contribution to the bulk stress. The squirming motion does affect the probability density distribution, which indirectly changes the bulk stress slightly. The apparent viscosity of a semi-dilute suspension of non-bottom-heavy squirmers is slightly smaller than that of inert spheres, and has a value very close to that given by (3.4) with $k = 5.0$ when $Sq = 1$ and $\beta = 5$. This result indicates that the effects of squirming motion and of Brownian motion on the apparent viscosity are similar. This is because both motions have the effect of preventing two particles from swimming (or moving) as a pair, though two inert spheres in a shear flow exhibit an infinite region of closed trajectories. In the case of strong Brownian motion, we can assume a homogeneous distribution of particles. The distribution is not homogeneous in the case of squirmers, so the effects of the two motions are not exactly the same.

A suspension of Brownian spheres generates an isotropic bulk stress, so it is very different from a suspension of *bottom-heavy* squirmers. In this case, the stresslet generated by the squirming motion is no longer isotropic and the squirming motion generates a strong direct contribution to the bulk stress at $O(c)$. When the gravitational direction is in the $-\boldsymbol{x}$-direction, while the background simple shear flow is in the x,y-plane, i.e. it is directed vertically, the apparent viscosity of the semi-dilute suspension of bottom-heavy squirmers becomes smaller than that of inert spheres. Moreover, it can even become smaller than the viscosity of the solvent fluid. It is also found that the suspension shows a considerable first normal stress difference. When the gravitational direction is in the $-\boldsymbol{y}$-direction, i.e. the shear flow is horizontal but varies vertically, the effect of squirming on the particle bulk stress is completely different from the previous case. The change in the gravitational direction induces the opposite effect of the squirming stresslet on H_{xy}, and hence increases the apparent viscosity. The first normal stress difference of the particle bulk stress has the opposite sign from the case with $\boldsymbol{g}/g = -\boldsymbol{x}$, and a substantial second normal stress difference appears when $\boldsymbol{g}/g = -\boldsymbol{y}$. In both cases, the parameters β and Sq enhance the effect of squirming on the particle bulk stress. The basic properties of the particle bulk stress, such as the sign of its components, are mainly dominated by the gravitational direction, G_{bh} and sign of β. When the gravitational direction is in the $-z$-direction, the effect of squirming on the rheology of the suspension is small, except for the second normal stress difference. Roughly speaking, however, the rheological effect for bottom-heavy squirmers is not due to cell–cell interactions, but due to the intrinsic stresslets on the aligned individual squirmers.

It is possible to compare the average velocity vectors of bottom-heavy squirmers with Kessler's (1986*a*) experiments using vertical pipe flow. The present numerical results show a tendency similar to the experiments: the squirmers are moving towards lower values of the upflow velocity. The average velocity vectors vary with parameters G_{bh}, Sq, β and c, but all the results obtained in this paper show similar tendencies. We may note that an individual cell (or squirmer) will tumble if the horizontal component of background vorticity is strong enough, but will still swim towards the region of minimum upflow on average (Kessler 1986*a*; Pedley & Kessler 1990). In the case of a solitary squirmer, it tumbles if $G'_{bh} < 4\pi$, which includes the case with $G_{bh} = 10$ and $Sq = 1$. In such cases, the lengths of the average velocity vectors are much shorter than one, because some of the squirmers tumble and their orientation has a wide distribution. The migration of cells may not appear if the cells' diffusive swimming motion, due to the tumbling and the hydrodynamic interaction between cells, overwhelms the average swimming motion of cells.

In this paper, we investigate rheological properties only in a simple shear flow. It would be more convenient if we could calculate the particle stress tensor in a general linear flow field, but we have not succeeded yet. A future step towards that goal will be to investigate an extensional flow, which is a well-known standard flow field. For isolated squirmers in an extensional flow field, the suspension rheology is very simple. There is no background vorticity in an extensional flow, so a non-bottom-heavy squirmer does not change its orientation with time, and a bottom-heavy squirmer orients itself upwards after a long enough time. The stresslet of a solitary squirmer with a certain orientation vector can be calculated from (1.4). In the case of a semi-dilute suspension of non-bottom-heavy squirmers, the stresslet generated by the squirming motion is isotropic, and it indirectly changes the bulk stress slightly. Inert spheres in an extensional flow have no closed trajectories, so we cannot tell from this study whether the squirming motion will reduce or increase the probability density

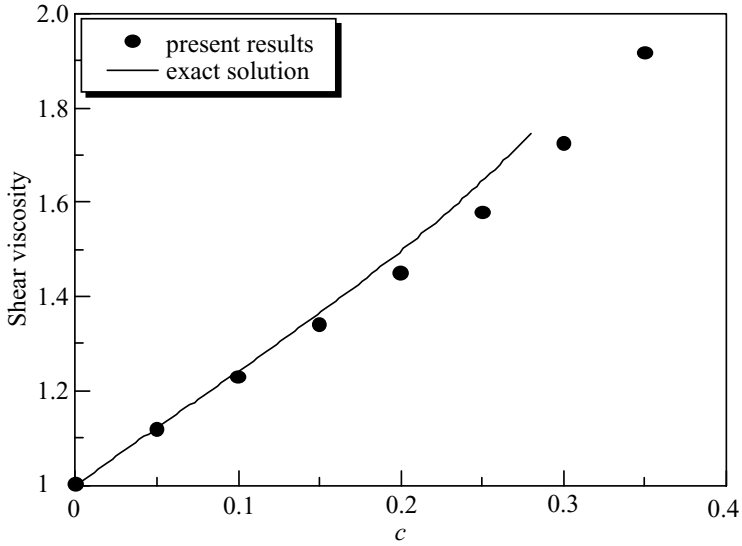

FIGURE 36. The shear viscosity for a suspension of rigid spheres placed on a simple cubic lattice. 'Present results' indicates the results obtained by the present numerical method using 64 spheres, and 'exact solution' indicates the exact solution obtained by Nunan & Keller (1984) considering the interaction between an infinite number of spheres.

in the near field, and whether it decreases or increases the extensional viscosity. In the case of a semi-dilute suspension of bottom-heavy squirmers, most of the squirmers will tend to orientate upwards because of the absence of background vorticity. The particle stress tensor is strongly dependent on the orientation, and the extensional viscosity is also strongly dependent on the relative direction of gravity to the extensional direction. The hydrodynamic interaction between cells tends to disperse the orientations of cells and to modify equation (1.4) for the stresslet. By increasing the interaction, i.e. increasing c or $|\beta|$, the non-Newtonian effects may be decreased, because the stresslet becomes more isotropic. The overall tendency in the case of an extensional flow is different from that of a shear flow, because of the difference in background vorticity, which will be a dominant factor in considering the rheology of cell suspensions.

T. I. was supported by a JSPS postdoctoral fellowship for research abroad from 2003 to 2005.

Appendix A. Comparison with the exact solution for the shear viscosity of a periodic suspension

The aim of this appendix is to clarify the reliability of the present numerical method by comparing with the exact solution for the shear viscosity of a periodic suspension. The results of the shear viscosity for a suspension of rigid spheres placed on a simple cubic lattice is shown in figure 36, where 'present results' indicates the results obtained by the present numerical method using 64 spheres, and 'exact solution' indicates the exact solution obtained by Nunan & Keller (1984) considering the interaction between an infinite number of spheres. We see that the two results correspond well in the semi-dilute regime.

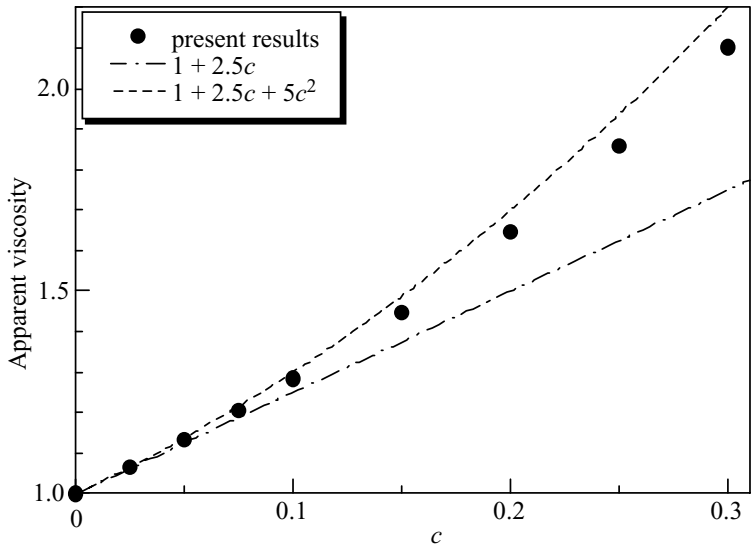

FIGURE 37. The apparent viscosity of a suspension of rigid spheres with the hard sphere distribution. 'Present results' indicates the viscosity calculated by the present numerical method. Batchelor's analytical solution is also shown.

Appendix B. Stresses in the case of the hard sphere distribution

The aim of this appendix is to show the stresses in a well-known microstructure, from which we expect that readers can have a feeling for the relative magnitude of the various contributions to the total stress. We use the hard sphere distribution here, because it is a well-known and easily reproducible microstructure. We performed the Monte Carlo simulations with 64 particles and 300 realizations, in which particles were laid down one by one, but a particle was removed if it overlapped an older particle. The stress components can be calculated by the present numerical method, and averaged over all realizations.

Figure 37 shows the apparent viscosity of a suspension of rigid spheres with the hard sphere distribution under a simple shear flow condition. Batchelor's analytical solution is also shown in the figure. We see that the present results show good agreement with Batchelor's analytical solution for $c \leqslant 0.1$.

REFERENCES

BATCHELOR, G. K. 1970 The stress system in a suspension of force-free particles. *J. Fluid Mech.* **41**, 545–570.

BATCHELOR, G. K. 1977 The effect of Brownian motion on the bulk stress in a suspension of spherical particles. *J. Fluid Mech.* **83**, 97–117.

BATCHELOR, G. K. & GREEN, J. T. 1972*a* The hydrodynamic interaction of two small freely-moving spheres in a linear flow field. *J. Fluid Mech.* **56**, 375–400.

BATCHELOR, G. K. & GREEN, J. T. 1972*b* The determination of the bulk stress in a suspension of spherical particles to order c^2. *J. Fluid Mech.* **56**, 401–427.

BEES, M. A. & HILL, N. A. 1998 Linear bioconvection in a suspension of randomly-swimming, gyrotactic micro-organisms. *Phys. Fluids* **10**, 1864–1881.

BLAKE, J. R. 1971 A spherical envelope approach to ciliary propulsion. *J. Fluid Mech.* **46**, 199–208.

BOSSIS, G. & BRADY, J. F. 1984 Dynamic simulation of sheared suspensions. Part I. General method. *J. Chem. Phys.* **80**, 5141–5154.

BRADY, J. F. & BOSSIS, G. 1985 The rheology of concentrated suspensions of spheres in simple shear flow by numerical simulation. *J. Fluid Mech.* **155**, 105–129.

BRADY, J. F. & BOSSIS, G. 1988 Stokesian dynamics. *Annu. Rev. Fluid Mech.* **20**, 111–157.

Brady, J. F., Phillips, R. J., Lester, J. C. & Bossis, G. 1988 Dynamic simulation of hydrodynamically interacting suspensions. *J. Fluid Mech.* **195**, 257–280.

Brenner, H. 1969 Rheology of a dilute suspension of dipolar spherical particles in an external field. *J. Colloid Interface Sci.* **32**, 141–158.

Childress, S., Levandowsky, M. & Spiegel, E. A. 1975 Pattern formation in a suspension of swimming micro-organisms: Equations and stability theory. *J. Fluid Mech.* **63**, 591–613.

Cichocki, B. & Felderhof, B. U. 1988*a* Short-time diffusion coefficients and high frequency viscosity of dilute suspensions of spherical Brownian particles. *J. Chem. Phys.* **89**, 1049–1054.

Dombrowski, C., Cisneros, L., Chatkaew, S., Goldstein, R. E. & Kessler, J. O. 2004 Self-concentration and large-scale coherence in bacterial dynamics. *Phys. Rev. Lett.* **93**, 098103.

Dratler, D. I. & Schowalter, W. R. 1996 Dynamic simulation of suspensions of non-Brownian hard spheres. *J. Fluid Mech.* **325**, 53–77.

Durlofsky, L., Brady, J. F. & Bossis, G. 1987 Dynamic simulation of hydrodynamically interacting particles. *J. Fluid Mech.* **180**, 21–49.

Einstein, A. 1906 Eine neue Bestimmung der Moleküldimensionen. *Ann. Phys.* **19**, 289–306.

Felderhof, B. U. & Jones, R. B. 2004 Small-amplitude swimming of a sphere. *Physica* A **202**, 119–144.

Guell, D. C., Brenner, H., Frankel, R. B. & Hartman, H. 1988 Hydrodynamic forces and band formation in swimming magnetotactic bacteria. *J. Theor. Biol.* **135**, 525–542.

Hatwalne, Y., Ramaswamy, S., Rao, M. & Simha, R.A. 2004 Rheology of active-particle suspensions *Phys. Rev. Lett.* **92**, 11801.

Hillesdon, A. J., Pedley, T. J. & Kessler, J. O. 1995 The development of concentration gradients in a suspension of chemotactic bacteria. *Bull. Math. Biol.* **57**, 299–344.

Ishikawa, T. & Pedley, T. J. 2007 Diffusion of swimming model micro-organisms in a semi-dilute suspension. *J. Fluid Mech.* **588**, 437–462.

Ishikawa, T., Simmonds, M. P. & Pedley, T. J. 2006 Hydrodynamic interaction of two swimming model micro-organisms. *J. Fluid Mech.* **568**, 119–160.

Jiang, H., Osborn, T. R. & Meneveau, C. 2002 Hydrodynamic interaction between two copepods: A numerical study. *J. Plank. Res.* **24**, 235–253.

Kessler, J. O. 1985*a* Hydrodynamic focusing of motile algal cells. *Nature* **313**, 218–220.

Kessler, J. O. 1985*b* Co-operative and concentrative phenomena of swimming micro-organisms. *Contemp. Phys.* **26**, 147–166.

Kessler, J. O. 1986*a* The external dynamics of swimming micro-organisms. In *Progress in Phycological Research*, Vol. 4 (ed. F. E. Round & D. J. Chapman), pp. 257–307. Biopress.

Kessler, J. O. 1986*b* Individual and collective dynamics of swimming cells. *J. Fluid Mech.* **173**, 191–205.

Kessler, J. O., Hoelzer, M. A., Pedley, T. J. & Hill, N. A. 1994 Functional pattern of swimming bacteria. In *Mechanics and Physiology of Animal Swimming* (ed. L. Maddock, Q. Bone & J. M. V. Rayner), pp. 3–12, Cambridge University Press.

Kim, S. & Karrila, S. J. 1992 *Microhydrodynamics: Principles and Selected Applications.* Butterworth–Heinemann.

Lega, J. & Passot, T. 2003 Hydrodynamics of bacterial colonies. *Phys. Rev.* E **67**, 031906.

Lighthill, M. J. 1952 On the squirming motion of nearly spherical deformable bodies through liquids at very small Reynolds numbers. *Commun. Pure Appl. Maths.* **5**, 109–118.

Magar, V., Goto, T. & Pedley, T. J. 2003 Nutrient uptake by a self-propelled steady squirmer. *Q. J. Mech. Appl. Maths.* **56**, 65–91.

Mehandia, V. & Nott, P. R. 2004 The collective dynamics of self-propelled particles (abstract). In *Proc. XXI ICTAM*, Poland, FM16L-10603.

Mendelson, N. H., Bourque, A., Wilkening, K., Anderson, K. R. & Watkins, J. C. 1999 Organised cell swimming motions in Bacillus subtilis colonies: Patterns of short-lived whirls and jets. *J. Bacteriol.* **180**, 600–609.

Metcalfe, A. M. & Pedley, T. J. 2001 Falling plumes in bacterial bioconvection. *J. Fluid Mech.* **445**, 121–149.

Metcalfe, A. M., Pedley, T. J. & Thingstad, T. F. 2004 Incorporating turbulence into a plankton foodweb model. *J. Marine Systems* **49**, 105–122.

Nasseri, S. & Phan-Thien, N. 1997 Hydrodynamic interaction between two nearby swimming micromachines. *Comput. Mech.* **20**, 551–559.

NOTT, P. R. & BRADY, J. F. 1994 Pressure-driven flow of suspensions: simulation and theory. *J. Fluid Mech.* **275**, 157–199.

NUNAN, K. C. & KELLER, J. B. 1984 Effective viscosity of a periodic suspension. *J. Fluid Mech.* **142**, 269–287

O'BRIEN, R. W. 1979 A method for the calculation of the effective transport properties of suspensions of interacting particles. *J. Fluid Mech.* **19**, 17–39.

PEDLEY, T. J. & KESSLER J. O. 1990 A new continuum model for suspensions of gyrotactic micro-organisms. *J. Fluid Mech.* **212**, 155–182.

PEDLEY, T. J. & KESSLER, J. O. 1992 Hydrodynamic phenomena in suspensions of swimming microorganisms. *Annu. Rev. Fluid Mech.* **24**, 313–358.

RAMIA, M., TULLOCK, D. L. & PHAN-THIEN, N. 1993 The role of hydrodynamic interaction in the locomotion of microorganisms. *Biophys. J.* **65**, 755–778.

STONE, H. A. & SAMUEL, A. D. T. 1996 Propulsion of microorganisms by surface distortions. *Phys. Rev. Lett.* A **77**, 4102–4104.